

BIOSENSOR DESIGN BASED ON IMMUNOBINDING-INDUCED
FLUORESCENCE POLARIZATION CHANGE AND QUANTUM
DOTS FLUROESCENCE QUENCHING BY GOLD
NANO-PARTICLES VIA BIOCONJUGATION

By

YANLING QIAO

A thesis submitted in partial fulfillment of
the requirements for the degree of

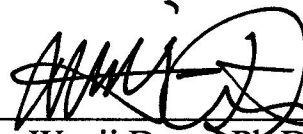
MASTER OF SCIENCE IN CHEMICAL ENGINEERING

WASHINGTON STATE UNIVERSITY
School of Chemical Engineering and Bioengineering


DECEMBER 2009

To the Faculty of Washington State University:

The members of the Committee appointed to examine the thesis of YANLING QIAO find it satisfactory and recommend that it be accepted.



Wenji Dong, Ph.D., Chair



Bernard J. Van Wie, Ph.D.



Prashanta Dutta, Ph.D.

ACKNOWLEDGMENT

I am deeply grateful to my advisor, Dr. Wenji Dong, for his guidance, encouragement and patience, without which I could not have achieved so much progress in research. I also thank the rest of my committee, Dr. Bernard J. Van Wie and Dr. Prashanta Dutta, for taking their time to review my thesis and participate in my final examination. I would like to acknowledge the financial support for this project from Life Science Discovery Fund (LSDF) of Washington State and the encouraging discussions with Dr. Cornelius Ivory.

I would like to thank Dr. Gerhard Munske in the Molecular Biology Core of Washington State University for synthesizing peptides and for valuable advice. I also thank Dr. Murali Chandra for kindly providing instruments in his lab.

I appreciate the generous help, active collaboration, and cherished friendship from postdoctoral scholars Dr. Yexin Ouyang and Dr. Jayant Jayasundar, graduate students Daniel C. Rieck and Zhiqun Zhou, and undergraduate students King Lun Li and Qingwen Xu in my lab.

I would like to thank all the people who have been helpful towards the completion of my degree, as well as the ones who provided support during my stay here at Washington State University.

Last but not least, I would like to thank my parents. Your love, support, encouragement and endless patience will always be inspirational for my entire life.

BIOSENSOR DESIGN BASED ON IMMUNOBINDING-INDUCED
FLUORESCENCE POLARIZATION CHANGE AND QUANTUM
DOTS FLUROESCENCE QUENCHING BY GOLD
NANO-PARTICLES VIA BIOCONJUGATION

ABSTRACT

by Yanling Qiao, M.S.
Washington State University
December 2009

Chair: Wenji Dong

Biosensors can recognize analytes, which are biomolecules or combined with biomolecules, by converting physiological data into detectable signals. Cardiac troponin I (cTnI) and cardiac troponin T (cTnT) have been drawing researchers' attention as markers for myocardial infarction due to their superior specificity and sensitivity for acute myocardial infarction. This thesis reports a novel dual-sensing scheme which is based on immunobinding-induced fluorescence polarization change in detection of these two cardiac markers. It also describes the efforts made in exploring the feasibility of using Förster resonance energy transfer (FRET) between gold nano-particles and quantum dots in biomarker sensing.

In the first design format, two small peptides corresponding to cTnI and cTnT were synthesized and labeled with different fluorescent dyes. After forming complexes with their antibodies, competition assays were performed in order to obtain standard curves

which could be applied in real sample analysis. Measurements were taken with increasing complexity from simple single peptide condition to mixed peptide in human plasma condition. The successful measurements at all conditions for both peptides demonstrate the good sensitivity, specificity, robustness, and promising potential applications in clinical diagnosis.

Luminescent quantum dots have distinctive properties over conventional organic fluorophores for their high quantum yield, size-tunable emission, broad absorption and narrow emission spectra, whereas gold nano-particles can induce strong fluorescence quenching of a fluorophore which is in a proximate distance. Using them as a FRET donor and acceptor pair in conjunction with the immunological interactions of biomolecules labeled on their surface, this system has shown effective sensing capability, and more than 50% of fluorescence was observed to be quenched at optimum testing conditions. Size of gold nano-particles, biotin to gold ratio, and biotinylated gold nano-particle to streptavidin conjugated quantum dot ratio were found to play important roles in regulating the system's quenching efficiency.

TABLE OF CONTENTS

	Page
ACKNOWLEDGMENTS.....	iii
ABSTRACT.....	iv
LIST OF TABLES.....	viii
LIST OF FIGURES.....	ix
CHAPTER	
1. Introduction.....	1
1.1 Heart Diseases and Acute Myocardial Infarction (AMI).....	1
1.2 Cardiac Troponin Complex Structure and Functions.....	1
1.3 Biochemical Markers for Heart Diseases	3
1.4 Cardiac Troponin Assay Methods Review.....	4
1.5 References.....	10
2. Sensor Design Based on Immunobinding-Induced Fluorescence Polarization Change.....	13
2.1 Introduction.....	13
2.2 Experimental Section.....	22
2.3 Results and Discussion.....	28
2.4 Conclusions.....	38
2.5 References.....	39
3. Sensor Design Based on Quantum-dots Fluorescence Quenching by Gold Nano-particles.....	40

3.1 Introduction.....	40
3.2 Experimental Section.....	46
3.3 Results and Discussion.....	53
3.4 Conclusions.....	64
3.5 References.....	64
4. Summary.....	66

LIST OF TABLES

Table 2.1	Fluorescence polarization values increase upon formation of antibody-peptide complexes.....	32
-----------	---	----

LIST OF FIGURES

Figure 2.1	Effects of polarized excitation and rotational diffusion on polarization of emission.....	14
Figure 2.2	Schematic layout of L-format FP measurement.....	19
Figure 2.3	Technical diagram and actual layout of ISS PC1 photon-counting spectrophotometer.....	20
Figure 2.4	Sensing scheme based on immunobinding induced fluorescence polarization change.....	21
Figure 2.5	ProTeam LC TM system 210.....	24
Figure 2.6	Fluorophore selection for dual detection scheme.....	27
Figure 2.7	Check hcTnI with SDS-PAGE during purification process.....	29
Figure 2.8	Immunoblotting of hcTnI.....	29
Figure 2.9	Check RcTnT with SDS-PAGE during purification process.....	30
Figure 2.10	Immunoblotting of RcTnT.....	30
Figure 2.11	Diagrams of competition assay at single peptide conditions.....	34
Figure 2.12	Diagrams of competition assay at mixed peptide conditions.....	36
Figure 2.13	Diagrams of competition assay at mixed peptide conditions with 10 time diluted human plasma.....	37
Figure 3.1	Schematic of quantum dot conjugate.....	43
Figure 3.2	Relative sizes of quantum dots, biomolecules, colloidal gold and cells...	43
Figure 3.3	Six different size quantum dots show different colors excited by a long-wave UV-lamp.....	44

Figure 3.4	Quantum dot 605 broad excitation and narrow, symmetric and Gaussian-like emission spectra, excited with 413 nm laser.....	44
Figure 3.5	Sensing scheme based on quantum dots quenching by gold nano-particles via bioconjugation.....	47
Figure 3.6	Chemical structure of biotin-HPDP.....	49
Figure 3.7	Transmission electron micrograph of gold nano-particles.....	52
Figure 3.8	Kinetics of BSA surface sylvhydryl blocking by NEM.....	54
Figure 3.9	Absorption spectrum of 20 nm bare gold nano particles and 20 nm biotinylated gold nano particles.....	56
Figure 3.10	Color comparison of different biotin-HPDP vs. gold nano-particles ratio in biotinylation.....	56
Figure 3.11	Biotin-HPDP concentration effects on the fluorescence quenching efficiency.....	57
Figure 3.12	Gold nano-particles size effects on fluorescence quenching efficiency...	58
Figure 3.13	Effects of NEM-BSA phosphate buffer dilution on the fluorescence quenching efficiency.....	61
Figure 3.14	Fluorescence recovery after adding sodium cyanide.....	63
Figure 3.15	Quenching test at different biotinylated GNPs vs. SQdot 605 ratio.....	63

Chapter 1

Introduction

1.1 Heart disease and acute myocardial infarction (AMI)

Heart disease ranks top on the list of the most serious health problems in United States, and statistics show that 1.5 million heart attacks occur in the United States each year, leading to about 500,000 deaths. Coronary heart disease is the most common type of all heart problems, and it is also the leading cause of heart attack. Heart attack is also known as acute myocardial infarction (AMI), whose symptoms include chest pain, spreading pain to shoulders, neck or arms, vomiting, nausea, paleness, and increased or irregular heart rate.

The World Health Organization has established its criteria for AMI diagnosis. These include an elevated cardiac markers level accompanied by either typical symptoms (such as chest pain) or diagnostic electrocardiographic changes.

The timely diagnosis and risk stratification of AMI are very essential in saving patients' lives and decreasing the mortality rate caused by heart disease. This issue has been drawing the researchers' attention all the time. The early and accurate detection of cardiac biomarkers for heart failure in human blood serum is among the hottest topics of all. One of the important cardiac biomarkers is cardiac troponin, which plays a central role in regulation of cardiac contraction.

1.2 Cardiac Troponin complex structures and functions

Troponin complex was first described by Ebashi and Kodama in 1968 [1], and they showed that this special protein regulates the contraction of striated muscle but not smooth muscle. Cardiac troponin complex and contractile proteins including actin, myosin and tropomyosin compose cardiac sarcomere. Troponin complex is the central unit which regulates the interaction of the thin (actin and tropomyosin) and thick (myosin) filaments in the striated muscle in response to variation of the intracellular calcium concentration. As a component of thin filament, troponin is located within the groove between actin filaments in muscle tissue, and it is composed of three subunits: troponin C (TnC), troponin I (TnI), and troponin T (TnT). TnC is an 18 kDa subunit with calcium-binding properties, which regulates the activation of thin filament during contraction by producing conformational change and removing inhibition of TnI. Cardiac TnI (cTnI) is a 24 kDa inhibitory subunit which binds to actin in thin myofilaments to hold the troponin-tropomyosin complex in place. Cardiac TnT (cTnT) is a 37 kDa structural subunit that binds to tropomyosin, interlocking them to form a troponin-tropomyosin complex.

Cardiac TnC, TnI and TnT are called “cardiac troponins” because they are different from their skeletal muscle isoforms. Skeletal TnC has four Ca^{2+} binding sites, while cardiac TnC (cTnC) has only three. The inhibitory component TnI has three isoforms which are characteristic for fast and slow skeletal muscle and cardiac muscle respectively. Phosphorylation modulates interaction among the troponin components, and this is especially important for cTnI. Cardiac troponin I has two serine residues on the 23rd and 24th amino acid (Ser-23 and Ser-24) which can be phosphorylated. The phosphorylation

of the serine residues by cAMP-dependent protein kinase, protein kinase C, or protein kinase A causes a decrease in affinity of Ca^{2+} for the calcium-binding protein cTnC, leading to the inhibition of actin-myosin cooperation.

1.3 Biochemical markers for heart diseases

There are three commonly used biochemical markers in the diagnosis of an AMI, which are serum myoglobin, creatine kinase-MB isoenzyme (CK-MB), and troponin subunits. Classical temporal “rise and fall” pattern was seen on all the markers associated with acute myocyte necrosis and protein release. In general, myoglobin is released first, followed by CK-MB and troponin. Patients with a normal CK-MB level but elevated troponin level are considered to have sustained minor myocardial damage, whereas patients with elevations of both CK-MB and troponins are considered to have acute myocardial infarction. cTnI can be detected in human serum after 4-6 hrs of symptom onset and increases to peak value in 18-24 hrs; it is also found that serum troponin concentration typically remains elevated for up to 14 days following myocyte necrosis, compared to the elevation of CK-MB only for about 2-3 days. Another advantage of cTnI over CK-MB as a marker is that CK-MB lacks specificity for cardiac injuries and it can also be measured in injured skeletal muscle. [2]

Although CK-MB is still used, cTnT and cTnI are emerging as the most specific and sensitive indicators for the detection of myocardial injury due to their unique amino acid sequences and intracellular localization in the cardiomyocyte. cTnI and cTnT generally have similar sensitivity and specificity for the detection of myocardial injury. cTnI is

released into the bloodstream during the ischemic and non-ischemic cardiac injuries and can be detected using monoclonal antibodies with very high sensitivity. An elevated cTnI and cTnT level is helpful in identifying patients at increased risk for development of acute myocardial infarction, but it is important to note that cardiac troponins are markers of all heart muscle damage, not just myocardial infarction. Increased risk is related quantitatively to the serum troponin level. Unlike troponin I levels, troponin T levels may be elevated in patients with renal disease, polymyositis, or dermatomyositis. The troponin test also can help assist the clinician in therapeutic intervention and risk stratification.

1.4 Cardiac troponin assay methods review

In the development of cTnI detection assays, various monoclonal antibodies have been developed against the most immunoreactive regions to detect cTnI in human serum samples. But unfortunately, significant variability exists between these assay methods. Up to 20-fold variation of serum cTnI concentrations have been observed for a given patient sample when measured with different assay methods [3]. These differences are mainly caused by the lack of mass standardization, the presence of post-translationally modified cTnI in the serum, and differences in antibody cross-reactivities to the various detectable forms of cTnI. cTnT is believed to be free from such problems, but this remains to be proven. Only one commercially available cTnT assay has been developed and patented so far. The first attempt to measure cTnI concentration in patients was made in 1995 with first generation assay [4]. One characteristic of these assays is that the monoclonal antibodies have very high specificity for cardiac isoform without cross-reactivity with skeletal isoforms. But the problem is that detection of cTnI was affected

by several modifications after cTnI release into bloodstream, such as covalent complex formation, selective degradation, oxidation and phosphorylation.

Cardiac TnI often forms complexes with other troponin subunits. There is debate about the relative percentages of free and complexed cTnI, and the nature of these free and complexed forms. Using Western blot analysis, it has been shown that cTnI exists predominantly as free subunits [5]. But opposite results were obtained by another group using specific monoclonal antibodies, and cTnI is found to be released into the circulation largely as the cTnI-cTnC binary complex, with less than 10% free cTnI form [6]. Morjana reported that serum cTnI predominantly associated with cTnC and cTnT as a ternary complex [7]. Other investigators found that cTnI exists in serum primarily as a cTnI-cTnC binary complex, and free cTnI, the binary complex cTnI-cTnT, and the cTnI-cTnC-cTnT ternary complex are rarely present, and when present, exist in very small quantities compared to the binary cTnI-cTnC complex.

There is also evidence that the C- and N- termini of cTnI molecules are unstable and rapidly eliminated after AMI, and a more stable fragment from amino acid residue 30 to 110 is generated. These studies indicated that both the C- and N-termini of free cTnI are subject to proteolysis with C-terminus preferentially degraded. An 18 kDa fragment is detected in AMI patients' plasma samples, and it is confirmed to result from C-terminus degradation [7]. Due to the cTnI degradation pattern, assay methods that recognize the C-terminal portion of the molecule tend to give lower apparent troponin concentrations than the assays which recognize N-terminus. Moreover, cTnI in complex form is degraded

similarly, but more slowly compared to free cTnI. Many investigators have reported that the extent of degradation is related to the degree of ischemia. That is, the greater the ischemia, the more degradation. It is also found that in different patients' serum cTnI samples, the extent of degradation also appears to be different, and the difference to some extent contributes to the standardization of cTnI assay methods.

Therefore, the second generation cTnI assays have tried to take into account the free or complex form of cTnI, its post translational modifications and selective degradation, with the hope of providing more robust assays.

In the effort of detecting analytes of interest, various biosensors have been developed during the last two decades. The rapid advances of biosensing technologies will definitely contribute a lot in biological and medical diagnosis.

Based on the analyte recognition method, biosensors that involve antibody-antigen interactions, enzymatic interactions and nucleic acid interactions are the most common forms. Antibodies are proteins produced by animal body's immune system in response to foreign agents. These complex biomolecules have highly ordered amino acid sequences, hence highly specific binding capabilities to specific structures. Enzymes are good candidates for bioreceptors because of their specific binding capabilities and catalytic activity, which allow for much lower detection limits than common binding techniques. The highly accurate complementary pairing of base pairs provides the basis for the specificity of biorecognition of DNA biosensors.

As for the signal transduction units, they can be optical which measures fluorescence, absorption, surface plasmon resonance etc., electrochemical which measures the electric current resulting from the electrochemical redox reaction of working electrode and gas diffused onto it, and piezoelectric sensors which electrically measures the small mass change induced by the loss of symmetry structure of ionic bonded crystal when stressed [8, 9].

In the sensing design for cardiac troponin detection, the immunoassay is employed in most cases due to its high specificity and sensitivity. As for the signal transduction part, the optical signal is the most frequently used form to be detected, and it has been developing from end point sensing such as enzyme-linked immunosorbent assay (ELISA) and Förster resonance energy transfer (FRET) to real-time sensing methods which include the surface plasmon resonance (SPR) technique [10,11,12]. As part of the overall goal to produce a biosensor microarray for simultaneous detection of AMI markers, Regan et al. described the development of cTnI sensor based on the ELISA assay. They showed a 10-fold variation in detection limit for free cTnI and complexed cTnI with cTnC, and they fabricated an immunosensor for free cTnI in whole blood with detection limit of 1 ng/ml and a total assay time of 45 min [13]. With the distance-dependent energy transfer property, FRET is also one of the common signal transduction methods. Grant et al. designed an immunosensor using the FRET technique which can recognize both cTnI and cTnT, and they reported the detection limit of both antigens reaching a concentration level down to 27 nM [14]. Because the SPR sensor has the advantages of not requiring probe labeling, it reduces the preparation steps. With its combination of low cost and

real-time measurement features, it is a very widely used technique in cardiac marker detection. In some of the studies, gold nano-particles are used to enhance fluorescence signal artificially because of their high-density surface plasmon polariton fields, and a 3 to 4 times fluorescence signal enhancement was observed [15,16]. But the disadvantage of using the SPR technique is that the detection limit is restricted to 1-10 nM for the 20-kDa protein and even higher for smaller ones. It also requires protein immobilization onto the detection surface to avoid desorption caused by sample flowing [17].

Because not all molecules of interest are strongly fluorescent and fluorescent dye labeling is labor intensive, electrochemical sensors are very complementary to fluorescent sensors for their rapid, simple, and low-cost field detection. Electrochemical sensors based on intrinsic redox-active amino acids, antibodies and aptamers have been developed and found applications.

Despite the extensive development of those sensors, each design has its own strengths and disadvantages. Optical sensors are based on SPR and ELISA, and electrochemical sensors require the immobilization of recognition molecules on sensing plates, while FRET technique requires fluorescent dye labeling on both donors and acceptors. Therefore, it is highly desirable to develop sensors with fewer preparation steps but that still provide uncompromising sensitivity and reliability. Peptide-based fluorescence polarization immunoassay has the characteristics of in-solution detection, only labeling one molecule and high sensitivity, which make it a promising candidate. Quantum dots and gold nano particles are becoming more and more popular as fluorescence donor-

acceptor pair for their high quantum yield and strong quenching capability respectively; quantum dots also make multiple analytes detection possible with their narrow emission spectra. Currently no research has been reported on the detection of cTnI and cTnT with these two sensing techniques; we would like to explore the feasibility of implementing these two techniques in the detections of cTnI and cTnT from serum plasma.

Our long-term goal is to explore and develop a sensitive and reliable sensing scheme which can be applied in the detection of human cTnI (hcTnI) and cTnT (hcTnT) *in vitro*. Easy fabrication, fast detection, simple and straightforward readout, and reliable testing results will be the features we expect to see on this sensor. The overall objective of this thesis is to test the sensing ideas which are based on immunobinding-induced fluorescence polarization change and quantum dots quenching by gold nano-particles via bioconjugation respectively.

Specifically, in the first design format which uses fluorescence polarization, we aim to monitor binding events in solution by observing fluorescence polarization value change of synthesized peptides which are labeled with fluorescence probes. The use of monoclonal antibody provides the possibility for analytes competition assay (full length proteins compete with the synthesized peptides for monoclonal antibody). The working hypothesis of this sensing design is that because the full length proteins have higher binding affinity to antibodies than peptides do, the competition assay will result in fluorescence polarization changes.

In the second design format which uses quantum dots and gold nano-particles as FRET donor and acceptor pair, we aim to report the analyte detection by the fluorescence intensity quenching upon the bioconjugation of biomolecules labeled on the surfaces of fluorescence donor quantum dots and quencher gold nano-particles. This process is based upon the hypothesis that the close proximity between the donor and acceptor resulted from antibody-antigen interaction will significantly quench the donor fluorescence.

1.5 References

- [1] Katus, H.A., Remppis, A., Looser, S., Hallermeier, K., Scheffold, T., Kubler, W. "Enzyme Linked Immunoassay of Cardiac Troponin T for the Detection of Acute Myocardial Infarction in Patients," *J Mol Cell Cardiol* 1989; 21:1349-1353.
- [2] Jillian, R. T. "Troponin Revisited 2008: Assay Performance," *Clin Chem Lab Meth* 2008; 46(11):1489-1500.
- [3] Wu, A.H., Feng, Y.J., Moore, R., Apple, F.S., McPherson, P.H., Buechler, K.F., Bodor, G. "Characterization of Cardiac Troponin Subunit Release into Serum after Acute Myocardial Infarction and Comparison of Assays for Troponin T and I," *Clin Chem* 1998; 44:1198-1208.
- [4] Missov, E., Calzolari, C. "Elevated Cardiac Troponin I in Some Patients with Severe Congestive Heart Failure," *J Mol Cell Cardiol* 1995; 27:A405, (Abstract).
- [5] Lavigne, L., Waskiewicz, S., Pervaiz, G., Fagan, G., Whiteley, G. "Investigation of Serum Troponin I Heterogeneity and Complexation to Troponin T," *Clin Chem* 1996; 42: S312, (Abstract).
- [6] Katrukha, A.G., Bereznikova, A.V., Esakova, T.V., et al. "Troponin I is Released in Bloodstream of Patients with Acute Myocardial Infarction Not in Free Form but as Complex," *Clin Chem* 1997; 43:1379–1385.

- [7] Morjana, N. "Degradation of Human Cardiac Troponin I after Myocardial Infarction," *Biotechnol Appl Biochem* 1998; 28:105-111.
- [8] Tuan, V. D., Brian, C., Fresenius, J. "Biosensors and Biochips: Advances in Biological and Medical Diagnostics," *Anal Chem* 2000; 366 :540–551.
- [9] Mundelanji, V., Kagan, K., Eiichi, T. "An Overview of Label-free Electrochemical Protein Sensors," *Sensors*. 2007; 7: 3442-3458.
- [10] Wei, J., Mu, Y., etc. "A Novel Sandwich Immunosensing Method for Measuring Cardiac Troponin I in Sera," *Anal Biochem* 2003; 321: 209-216.
- [11] Dutra, R.F. et al. "Surface Plasmon Resonance Immunosensor for Human Cardiac Troponin T Based on Self-Assembled Monolayer," *Journal of Pharmaceutical and Biomedical Analysis* 2007; 43:1744-1750.
- [12] Jin, W., Mu, Y., Jin, Q., Song, D., Wei, J., Zhang, H., Lin, X., "An Optical Immunosensor Based on Surface Plasmon Resonance for Human cTnI Determination Bioinformatics and Biomedical Engineering," 2008. ICBBE 2008. The 2nd International Conference on 16-18 May 2008 Page(s):1628 - 1631
- [13] Regan, T. O., Pravda, M., Sullivan, C. K., Guilbault, G. G. "Development of Biosensor Array for Rapid Detection of Cardiac Markers: Immunosensor for Detection of Free Cardiac Troponin I," *Anal Letters* 2003; 36(9):1903-1920.
- [14] Grant, S.A., Pierce, M.E., Lichlyter, D.J., Soykan, O. "Investigation of a FRET Immunosensor Technique for the Detection of Troponin T and I," *Sensor letters* 2004; 2: 58-63.
- [15] Wang, J., Hong, B., et al. "Mini Sensing Chip for Point-of-care Acute Myocardial Infarction Diagnosis Utilizing Micro-electro-mechanical System and Nano-technology," *Advances in experimental medicine and biology* 2009; 645:101-107.

- [16] Hong, B., Kai, J. et al. "Highly Sensitive Rapid, Reliable, and Automatic Cardiovascular Disease Diagnosis with Nanoparticle Fluorescence Enhancer and Mems," *Advances in experimental medicine and biology* 2008; 614:265-273.
- [17] Englebienne, P., Hoonacker, A. V., Verhas, M. "Surface Plasmon Resonance: Principles, Methods and Applications in Biomedical Sciences," *Spectroscopy* 2003; 17:255-273.

Chapter 2

Sensor design based on immunobinding-induced fluorescence polarization change

2.1 Introduction

Light can be considered as oscillations of an electromagnetic field perpendicular to the direction of propagation. Although both electric and magnetic components are present, we are concerned with the electric field. The electric field vector can be represented in an X-Y plane. The common light sources emit electromagnetic waves as a collection of all orientations of the emitters, which are depolarized, whereas the oscillation of X and Y components at the same phase results in an oscillation in a defined orientation that depends on the relative amplitude of each component. In this condition, the light is called linearly polarized.

Molecular electronic transitions are described in quantum mechanics by vectors in the physical space denoted as transition moments. The transition moments have a defined orientation with respect to the molecular axis. In an isotropic solution, the fluorophores are oriented randomly. Upon excitation with polarized light, fluorophores preferentially absorb photons whose electric vectors are aligned parallel to the transition moment of the fluorophore, and the ones whose absorption transition dipole is parallel to the electric vector of the excitation are selectively excited. This selective excitation results in a partially oriented population of fluorophores and in partially polarized fluorescence emission. This phenomenon is known as photoselection (Figure 2.1). Fluorescence

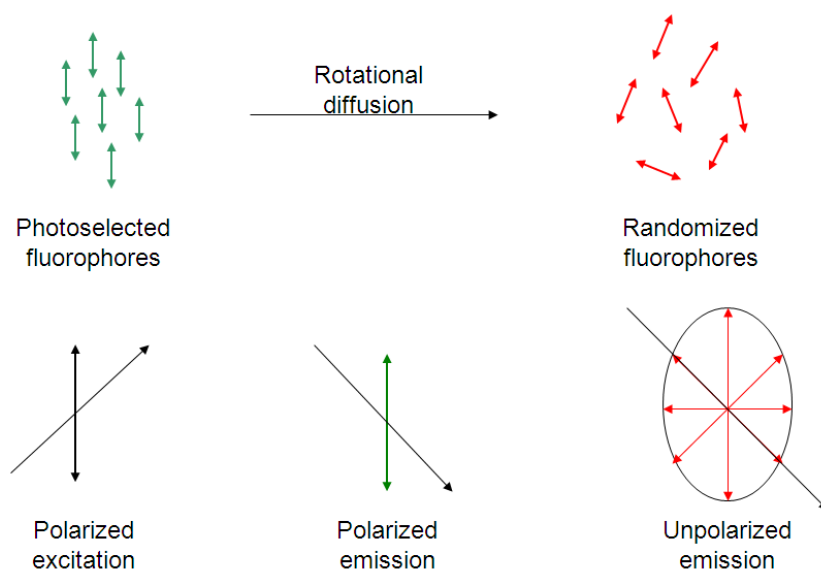


Figure 2.1 Effects of polarized excitation and rotational diffusion on polarization of emission [6]

polarization experiments are based on the principle of photoselective excitation of fluorophores by polarized light.

Fluorescence polarization (FP), first described by F. Weigert in 1920, [1] is based on the observation that when fluorescent molecules in solution are excited with plane-polarized light, they will emit light back into a fixed plane if the molecules remain stationary during the excitation process. Fluorescence is the process of photon emission as a result of the return of an electron in a higher energy orbital back to a lower orbital. The average time emitting molecules spend in the excited state prior to returning to the ground state, which is defined as the average fluorescence lifetime, ranges from 10^{-5} to 10^{-8} seconds, while the absorption that a photon in the process of excitation takes on is in the order of 10^{-15} seconds. Therefore, the significant time delay between absorption and fluorescence makes it possible for the molecule or its constituent parts to undergo noticeable positional displacement. When fluorescent molecules in solution are excited with polarized light, the degree to which the emitted light retains polarization reflects the rotation that the fluorophore undergoes during the interval between absorbance and subsequent emission.

Emission also occurs with the light polarized along a fixed axis in the fluorophore. The angle between these fixed orientations defines the maximum measurable anisotropy. The equation used to define fluorescence anisotropy is

$$r = \frac{I_{\parallel} - I_{\perp}}{I_{\parallel} + 2I_{\perp}} \quad (1)$$

While the polarization is:

$$P = \frac{I_{\parallel} - I_{\perp}}{I_{\parallel} + I_{\perp}} \quad (2)$$

where I_{\parallel} is the fluorescence intensity of vertically polarized emission (in which the two polarizers are parallel) and I_{\perp} is the intensity of horizontally polarized emission (in which the two polarizers are perpendicular to each other), and they both refer to the emissions when the sample is excited by vertically polarized light. The total fluorescence intensity I can also be determined from the same data with the equation $I = I_{\parallel} + 2I_{\perp}$.

Anisotropy (r) and polarization (P) are both expressions for the same phenomenon, and they can be interconverted using the equations:

$$P = \frac{3r}{2 + r} \quad (3)$$

$$r = \frac{2P}{3 - P} \quad (4)$$

As a ratio of emission light intensities, polarization is a dimensionless entity and does not depend on the intensity of the emitted light or the concentration of the fluorophore. Theoretically, the range of FP value is -0.1~0.5; negative polarizations are possible only if the perpendicular intensity exceeds the parallel intensity. Experimentally, the polarization value observed falls into the range from 0.03-0.3. This window of FP signal is sufficient, because the ratiometric FP signal is highly reproducible. While the robustness of the assay depends on the magnitude of the signal-to-noise ratio in other assays, in the FP assay the difference between highest signal and lowest signal (ΔP) is essential. An FP assay in which $\Delta P=0.1$ is considered a good assay, and one in which $\Delta P \geq 0.2$ is considered robust assay. [7]

In 1926, Perrin proposed that depolarization of fluorescence can be caused by rotational diffusion (Figure 2.1) and postulated that the polarization of luminescence is related to intrinsic polarization of the molecule and rotational diffusion by the following Perrin equation:

$$r = \frac{r_0}{1 + \tau / \phi} \quad (5)$$

Where r_0 is the anisotropy without effects of diffusion, τ is the fluorescence lifetime, and Φ is the rotational correlation time of the fluorophore. In a fluorescent conjugate that behaves as a rigid rotator in solution, the parameters r_0 and τ depend on the photophysical properties of the fluorophore, whereas Φ depends mainly on the size and shape of the macromolecule. This equation predicts that, when $\tau \ll \Phi$, the particle would almost not rotate at all during the lifetime of the fluorophore, and r approaches the anisotropy measured in the absence of diffusion, that is r_0 . On the other hand, when $\tau \gg \Phi$, the emission dipoles of the molecule become randomly distributed as a consequence of the rotational diffusion, and r approaches 0. The anisotropy will be sensitive to factors affecting the rotational motions when $\tau \approx \Phi$.

The polarization value of a molecule is proportional to the rotational relaxation (correlation) time of the molecule and is described by the Stokes equation

$$\phi = \frac{3\eta V}{RT} \quad (6)$$

where Φ is rotational relaxation time (the time required rotating through 68.5°), η is viscosity of the medium, V is the molecular volume of the molecule, R is the gas constant, and T is the temperature. Therefore, if viscosity and temperature are held constant,

polarization is directly proportional to molecular volume. Polarization and anisotropy are commonly used to describe molecular interactions in solution. If the fluorescent molecule is small, it rotates or tumbles faster in the aqueous solution and the resulting emitted light is random with respect to the plane of polarization (depolarized) and will have a lower FP value; if the fluorescent molecule is large, it remains relatively stationary and the emitted light will remain polarized and a higher FP value will be seen.

Fluorescence polarization assay is a versatile technique based on FP measurements, and it is now extensively used in various applications. Fluorescence polarization is mostly used in measuring equilibrium binding, nucleic acid hybridization, enzymatic activity, fluorophore concentrations, pH, and in study of molecular structure, binding events, and rotational diffusion. [3,4,5] It is more robust than conventional intensity measurements due to its ratiometric nature, and to some extent it is not sensitive to fluctuations in concentration, light source, or sample thickness. [2] Fluorescence polarization assays are carried out in homogeneous samples which do not require separation and do not require attachment to an immobilized phase. Because fluorescence polarization is rapid and the sample is not damaged during the measurement in aqueous sample, it can be measured repeatedly and after adding reagents.

There are two methods commonly used for steady state measurements of anisotropies, L-format (Figure 2.2) and T-format. In the L-format method, a single emission channel is used. The T-format makes use of separate channels in which the parallel and perpendicular components are observed simultaneously. The two methods have different

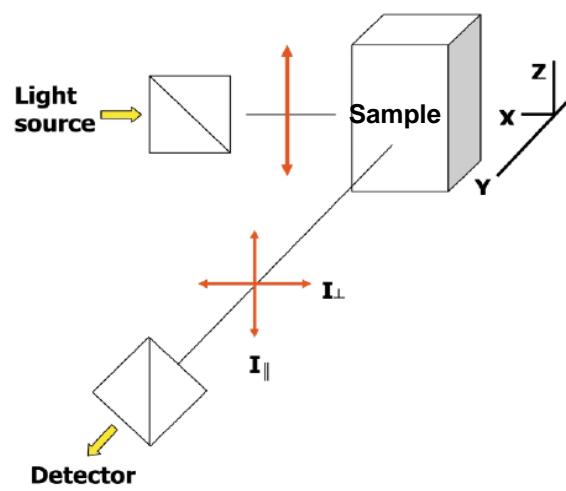


Figure 2.2 Schematic layout of L-format FP measurement [8]

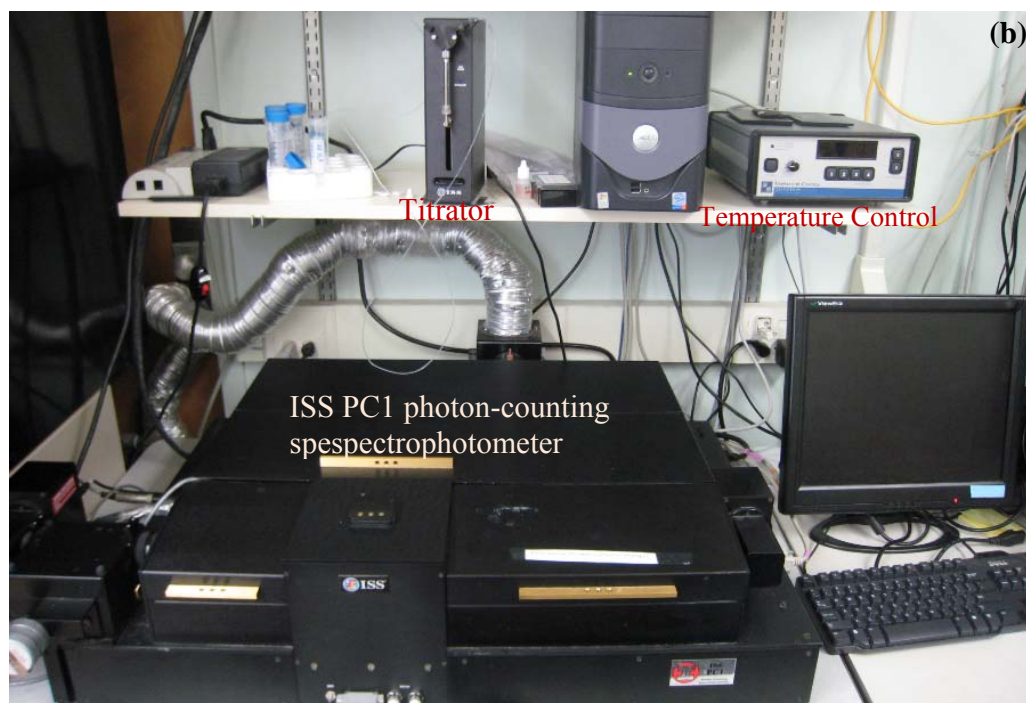
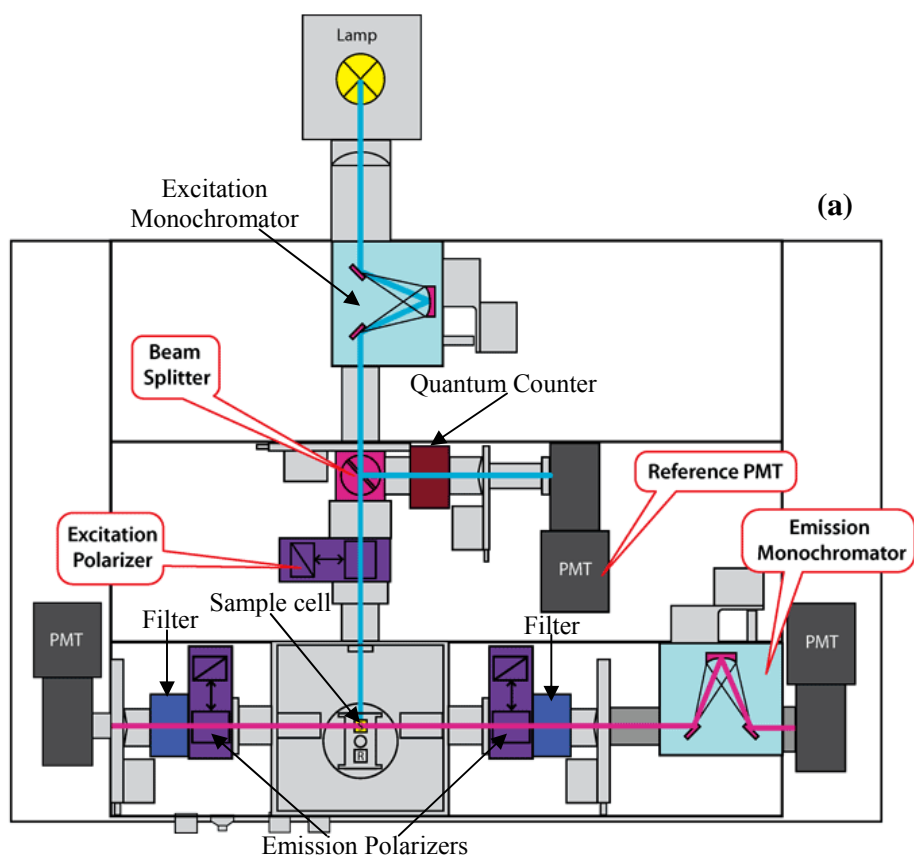


Figure 2.3 Technical diagram (a) and actual layout (b) of ISS PC1 photon-counting spectrophotometer

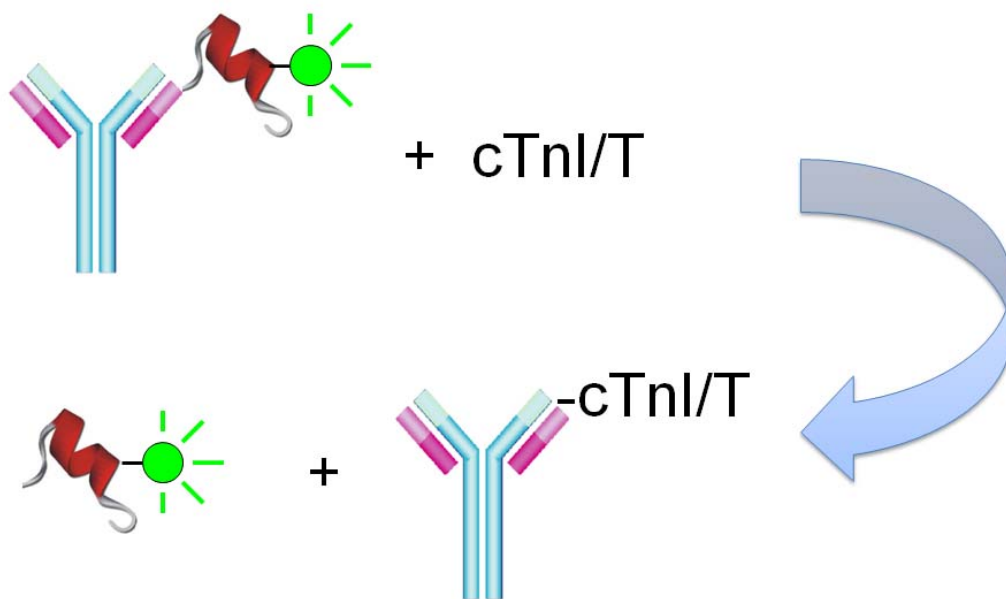


Figure 2.4 Sensing scheme based on immunobinding-induced fluorescence polarization change. Full-length proteins compete and displace synthesized peptide which will change the sample's FP value correspondingly

efficiencies for detecting various polarized components of fluorescent emission. The L-format is the most frequently used because most spectrophotometers tend to have one emission channel.

In this study, we aim to design a dual-sensing system which can detect the existence of two different cardiac disease markers *in vitro* from the same blood sample. As shown in figure 2.4, we will start with two synthesized peptides which are labeled with different fluorescent dyes. These two peptides contain the epitope region that can be recognized by cTnI and cTnT antibodies respectively. Here we hypothesize that since full-length proteins have higher binding affinity to their corresponding antibodies than fragment proteins do, in a competition assay, full-length proteins will be able to compete and displace the small peptides bound on antibody. Because the small peptides tumble much more readily in aqueous solution than they do when bound to much bigger antibody molecules, the fluorescence polarization value of the sensing system is expected to decrease upon the addition of full-length cTnI. Therefore it is possible to detect the existence of full-length cTnI and/or cTnT by measuring the fluorescence polarization values of analytes sample and comparing it with standard competition assay curve.

2.2 Experimental Section

Materials and reagents:

OneShot® BL21 Star™ (DE3) Chemically Competent *E. coli* cells were purchased from Invitrogen. 5-Carboxyfluorescein (5-FAM) was purchased from Sigma-Aldrich (St. Louis, MO). Texas Red®-X, succinimidyl ester (mixed isomers) was purchased from Invitrogen

Corporation (Carlsbad, CA). Peptides were synthesized by Molecular Biology Core of Washington State University. Mouse monoclonal cardiac troponin I antibody (ab19615) was obtained from Abcam (Cambridge, MA). Mouse monoclonal cardiac troponin T antibody (NB120-10213) was purchased from Novus Biologicals (Littleton, CO).

Wild type human cardiac troponin I (hcTnI) purification

Transform 0.2 μ l pET3d human cTnI into 20 μ l OneShot[®] BL21 Star[™] (DE3) Chemically Competent *E. coli* cells. Let it grow on LB agar plate at 37 °C overnight. Pick up several colonies; put them into 15ml TB medium with 50 μ g/ml carbenicillin and shake at 37 °C for 4 hrs. Inoculate the preculture into 2 L TB medium with 50 μ g/ml carbenicillin. After shaking at 37 °C for 18 hrs, spin down the cells at 7,000 rpm for 8 min. Suspend cell pellets with 200 μ l Triton X-100, 200 μ l 1% NaN₃, 1ml of 200 mM PMSF and 1 ml of 200 mM Benzamidine. Sonicate it with Misonix Sonicator[®] 3000 Ultrasonic Liquid Processor on ice for 15 min. Centrifuge the crude lysate at 20,000 rpm for 30 min. Then bring the supernatant to 30% and 60% saturation with (NH₄)₂SO₄ sequentially, followed by gently stirring at 4 °C for 1 hr and spinning down at 15,000 rpm for 20 min. Decant the supernatant and resuspend the pellet in 50 ml CM buffer. Dialyze against 1 L CM buffer overnight at 4 °C to remove residual (NH₄)₂SO₄. Load dialyzed supernatant into equilibrated carboxy methyl (CM) sepharose column and use ProTeam LC[™] System 210 (Figure 2.5) to run gradient elution with NaCl concentration increasing from 0 to 0.3 M. The eluted protein was monitored by absorbance, and each 8 ml was collected in culture tubes. Pick up the potential peak fractions from collection tubes and run sodium dodecyl sulfate polyacrylamide gel electrophoresis (SDS-PAGE) to



Figure 2.5 ProTeam LC™ System 210 (from Isco, Inc. picture from installation and operation guide)

find target protein. Pool the purified fractions and concentrate it.

Wild type rat cardiac troponin T (RcTnT) purification

Transform 0.2 μ l pSBETa RcTnI into 20 μ l OneShot® BL21 Star™ (DE3) Chemically Competent *E. coli* cells (from Invitrogen Corporation). Let it grow on LB agar plate at 37 °C overnight. Pick up several colonies; put them into 15 ml TB medium with 30 μ g/ml kanamycin and shake at 37 °C for 4 hrs. Inoculate the liquid preculture into 2 L TB medium with 30 μ g/ml kanamycin. After shaking continuously at 37 °C for 20 hrs, spin down the cells at 7,000 rpm for 8 min. Suspend cell pellets with 200 μ l Triton X-100, 200 μ l 1% NaN₃, 1 ml of 200 mM PMSF and 1 ml of 200 mM Benzamidine. Sonicate it with Misonix Sonicator® 3000 Ultrasonic Liquid Processor on ice for 15 min. Centrifuge the crude lysate at 20,000 rpm for 30 min. Then bring the supernatant to 30% and 60% saturation with solid ammonium sulfate sequentially, followed by gently stirring at 4°C for 1 hr and spin down at 15,000 rpm for 20 min. Decant the supernatant and resuspend the pellet in 50 ml DEAE buffer. Dialyze against 1 L DEAE buffer overnight at 4 °C to remove residual ammonium sulfate. Load dialyzed supernatant into diethylaminoethyl (DEAE) sepharose column and use ProTeam LC™ System 210 to run gradient elution with NaCl concentration increasing from 0 to 0.5 M. The eluted protein was monitored by absorbance, and each 8 ml was collected in culture tubes. Pick up the potential peak fractions from collection tubes and run sodium dodecyl sulfate polyacrylamide gel electrophoresis (SDS-PAGE) to find target protein. Pool the purified fractions and concentrate it.

Peptide synthesis and labeling

Two peptides were synthesized by Molecular Biology Core in Washington State University. The first peptide is a 15 amino acid sequence from 40th to 54th amino acid of full length human cTnI sequence, where the epitope region of corresponding antibody is from 41st to 49th amino acid. Both dephosphorylated and phosphorylated full length hcTnI will be able to compete with this peptide, that is, this peptide is designed for detection of total cTnI. The second peptide is a 19 amino acid sequence from 145th to 163rd amino acid of full length human cTnT sequence, where the epitope region of corresponding antibody is from 146th to 160th amino acid. cTnT is expected to compete with this second peptide, and it is supposed to detect hcTnT. The sequences (starting from N-termini) in one letter abbreviation are: (A). KISASRKLQLKTLLL; (B). EKERQNRLAEERARREEEE. After synthesis the peptides were labeled with 5-FAM and Texas Red respectively on N-termini (Figure 2.6). After synthesis and labeling of peptides, labeled peptide was separated from unlabeled peptide with high performance liquid chromatography. After purification step, mass spectrometry was run to check the peptide sequences synthesis and labeling. Charts are not shown here.

Immunobinding test by checking FP change

The tests were performed on ISS PC1 photon-counting spectrophotometer at 10 °C. Samples were held in 3 ml (1 cm path length) standard quartz cuvette. The labeled peptides were dissolved in PBS buffer (pH=7.4) at 40 nM, and fluorescence polarization were checked at fixed excitation and emission wavelength for the specific fluorophores (λ_{ex} =480 nm and λ_{em} =530 nm for 5-FAM; λ_{ex} =592 nm and λ_{em} =621 nm for Texas Red).

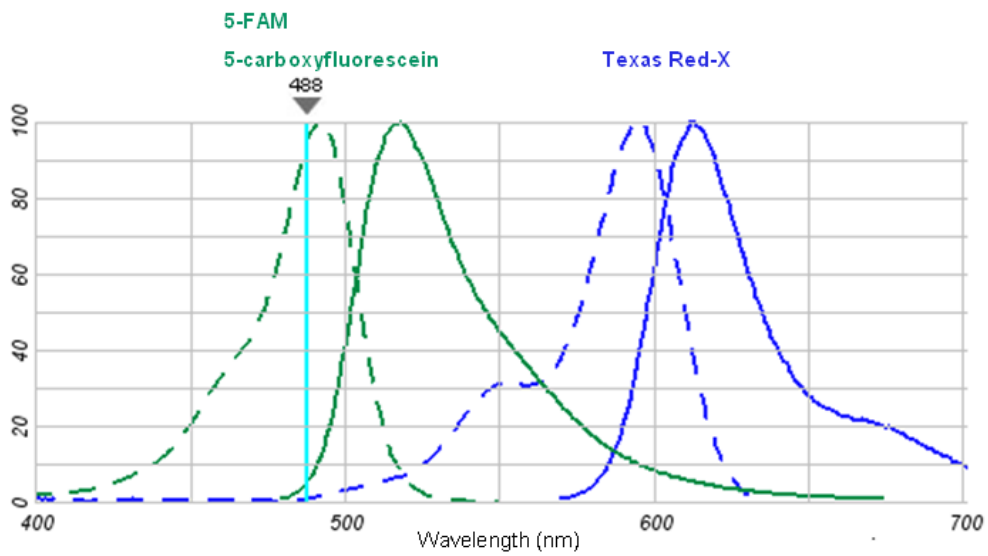


Figure 2.6 Fluorophores selection for dual detection scheme. Excitation and emission spectra are shown in dotted line and solid line respectively. (Adapted from online Fluorescence SpectraViewer on invitrogen® website.) 5-FAM and Texas Red are selected because of their well-separated emission spectra and documented uses in DNA/protein labeling

Because each antibody molecule has two binding sites, 20 nM antibodies were added to the peptide sample, and polarization value was measured again. Competition assay was carried out after establishing the base value of fluorescence polarization for peptide-antibody complex in sample preparations. The polarization changes were measured after addition of full-length proteins with increments of 5 nM until antibodies were saturated. The measurements were carried out at three different conditions for each peptide: 1) single protein detection in PBS buffer, 2) simultaneous detection of both cTnI and cTnT in PBS buffer, and 3) simultaneous detection of both cTnI and cTnT in the presence of human plasma. The fluorescence polarization values were obtained by averaging ten measured values of the sample at each condition. The two polarization values change were compared to see if antibody-peptide complexes were formed.

2.3 Results and discussion

Wild type human cardiac troponin I (hcTnI) purification

As shown in Figure 2.7(a), target protein hcTnI is seen in lanes 3, 4, 5, 7 and 8 as expected before passing CM column. Lane 6 also shows band of the same molecular weight, which could be caused by the residual supernatant on the surface of pellet during sampling. There is also small amount of target protein in lane 9 which is caused by the overflow from lane 8 while loading samples into the gel. In figure 2.7(b), the existence of impurity proteins is negligible compared to large amount of target protein shown in the potential peak.

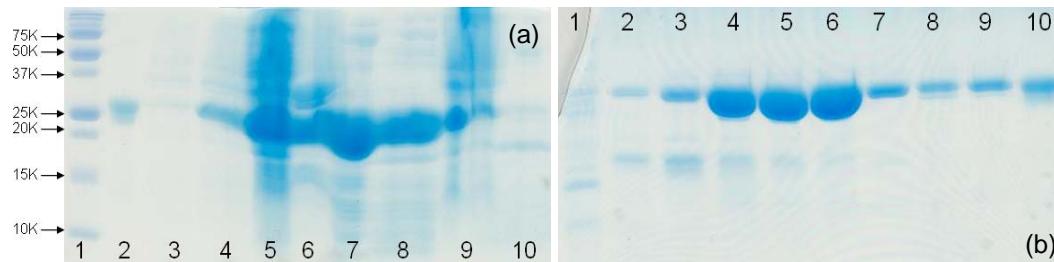


Figure 2.7 Check hcTnI with SDS-PAGE during purification process. (a) 1. BIO-RAD Precision Plus Protein all blue standards; 2. Standard human cTnI; 3. Preculture (4 hrs growth); 4. Supernatant after lysing & centrifugation; 5. Pellet 60% A.S. and dialysis against CM buffer overnight; 6. Pellet after lysing & centrifugation; 7. Pellet after 60% A.S. cut; 8. Supernatant after 30% A.S. cut; 9. Pellet after 30% A.S. cut; 10. Supernatant after 60% A.S. cut; (b) 1. Loading & washing pass through; 2-9. Check potential peak in different tubes; 10. Standard human cTnI

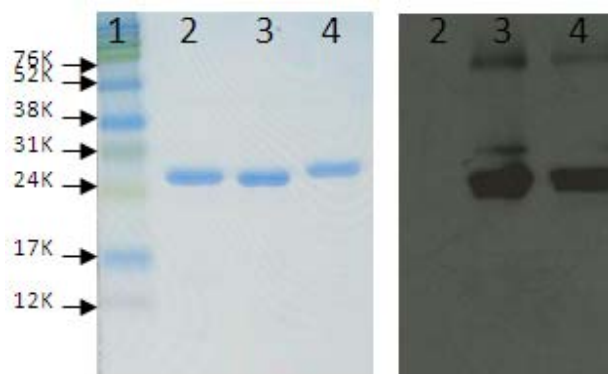


Figure 2.8 Immunoblotting of hcTnI. 1. Standard rainbow marker; 2. RcTnI; 3. purified hcTnI; 4. phosphorylated hcTnI

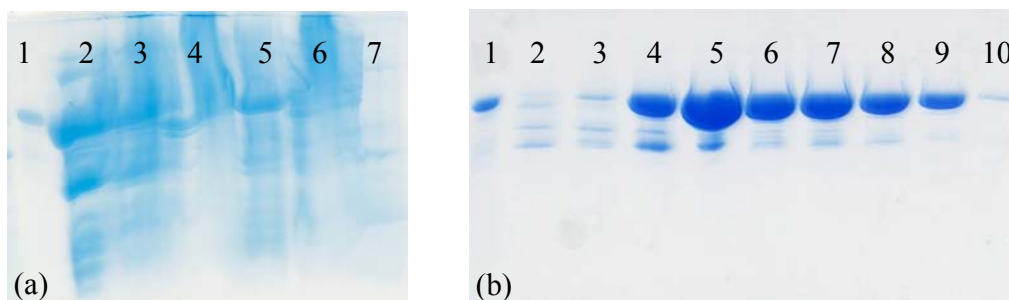


Figure 2.9 Check RcTnT with SDS-PAGE during purification process. (a) 1. Standard RcTnT; 2. Pellet after 60% A.S. cut and dialysis against DEAE buffer overnight; 3. Supernatant after lysing and centrifugation; 4. Pellet after lysing and centrifugation; 5. Supernatant after 30% A.S. cut; 6. Pellet after 30% A.S. cut; 7. Supernatant after 60% A.S. cut. (b) 1. Standard cTnT; 2-10. Check potential protein peak in fraction tubes from #47-#61

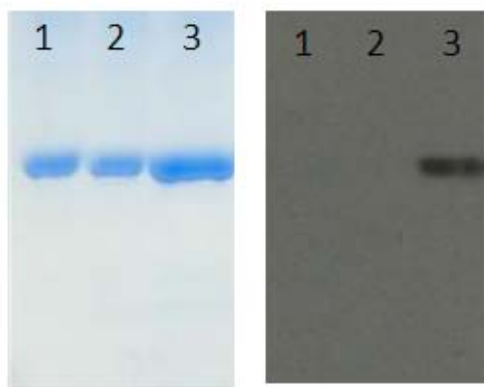


Figure 2.10 Immunoblotting of RcTnT. 1. RcTnT (181C); 2. RSTnT; 3. purified RcTnT (wt)

Immunoblotting was run after purification of hcTnI as shown in figure 2.8; bands are shown in target protein lane (3) and positive control lane (4), which further confirms the successful purification of hcTnI.

Wild type rat cardiac troponin T (hcTnT) purification

As shown in Figure 2.9(a), target protein RcTnT is seen in lanes 2, 3 and 5 as expected before passing DEAE column. In figure 2.9(b), more bands other than the target shown don't necessarily indicate more impurities since a freshly-made Coomassie Blue staining buffer which has higher sensitivity was used here.

Immunoblotting was run after purification of hcTnI as shown in figure 2.10; bands are shown in target protein lane (3) which proves the successful purification of RcTnT. The absence of positive control band might be caused by the mutagenesis on 181st amino acid even though this amino acid is not within the epitope region.

Sensing immunobinding by polarization measurements

The binding of each fluorophore-labeled peptide to the corresponding antibody (ab19615 from Abcam® for peptide A; NB120-10213 from Novus Biologicals® for peptide B) was investigated by monitoring fluorescence polarization changes of the peptide at different conditions. Significant increases in fluorescence polarization were observed when antibodies were added to each peptide sample (Table 2.1). These increases were induced by significant changes in molecular size before and after the small peptide (2~3 kDa) binding to large antibody (150 kDa). The binding increased the rotational correlation time,

Table 2.1 FP value increases upon formation of antibody-peptide complexes

	FP (peptide)	FP (ab-peptide complex)	FP increase (%)
Peptide only (A)	0.076	0.170	123.68
Peptide only (B)	0.0986	0.1511	53.24
Mixed peptides (A)	0.0651	0.1499	130.26
Mixed peptides (B)	0.1138	0.1675	47.19
Mixed peptides in human plasma (A)	0.1549	0.2143	38.35
Mixed peptides in human plasma* (B)	0.1243	0.1771	42.48

* In this particular test, up to 95% albumin and IgG were depleted from human plasma with HiTrap Albumin & IgG Depletion column (#28-9466-03 from GE Healthcare) because too strong background noises were seen in 10% human plasma solution.

which in turn led to larger polarization value according to Perrin equation. Generally, much larger increases in fluorescence polarization were observed for antibody-peptide A binding than antibody-peptide B binding at each condition. This is mainly because peptide A (2.088 kDa) has much lower molecular weight than peptide B (3.099 kDa). The heavier dye (641.15 g/mol Texas Red compared to 376.32 g/mol of 5-FAM on peptide A) tethered on the end of peptide B also contributed to the smaller FP change, since it is less likely to reflect the real-time movement of the peptide in aqueous solution.

Competition assays

In the sample which already contains antibody-peptide complexes, wild type full-length protein was added to compete with bound peptide. The hypothesis that full-length protein has higher binding affinity to antibody was confirmed because decreasing polarization values were seen with increasing amount of full-length proteins in both samples at all six conditions, either with or without external interfering factors. The portion of peptides which were displaced and released from the antibody with the existence of full-length protein contributed to the decreasing value of the sample. In all measurements, linear relationships of FP value with full-length protein concentration were obtained.

Figure 2.11 (a) and (b) show the single peptide competition assays and linear fittings of cTnI and cTnT. While both demonstrate good linearity with coefficient of determination close to 1 ($R^2=0.9638$ for figure a and $R^2=0.9643$ for figure b), cTnI competition assay gives larger slope (-0.0013 compared to -0.0012 of cTnT) and hence better sensitivity and resolution, which is also consistent with the previous results in antibody-peptide

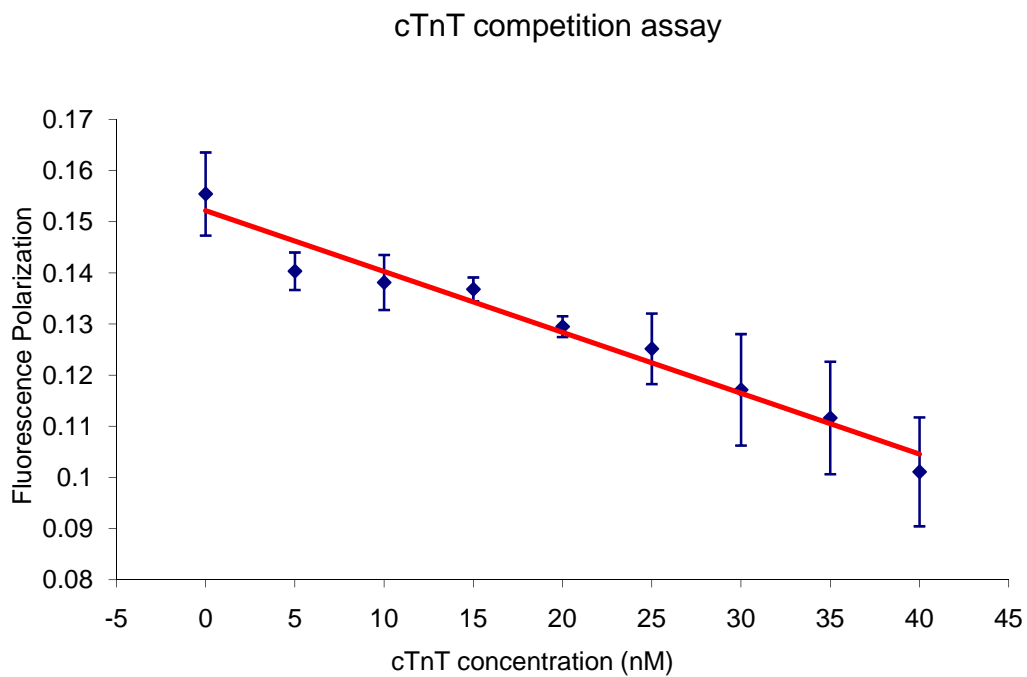
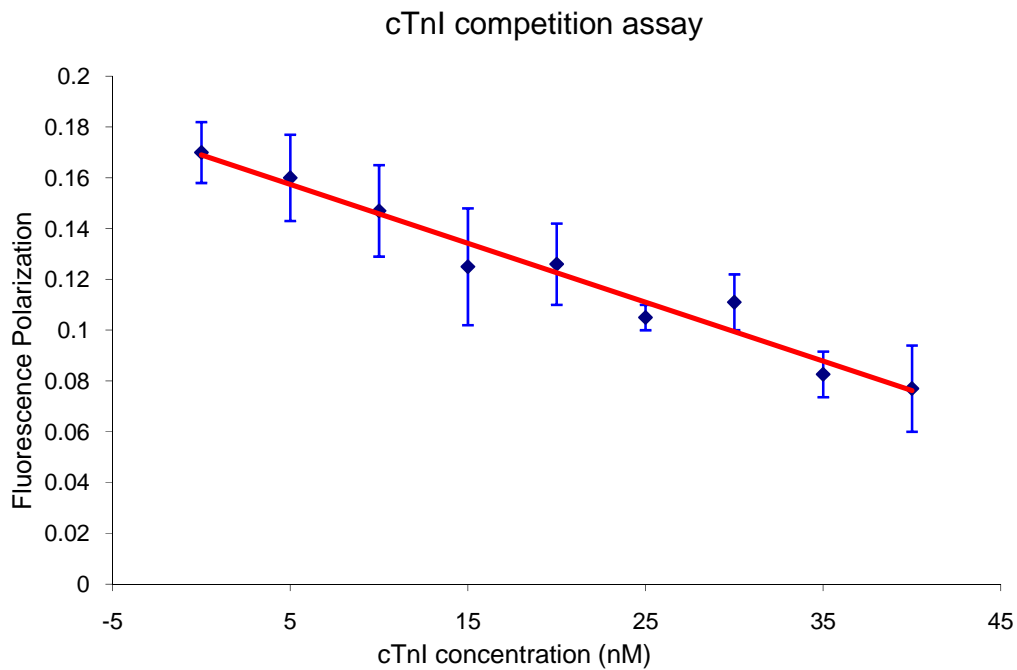


Figure 2.11 Diagrams of competition assay at single peptide conditions. Square dots are data points, red line is linear fitting, and error bars are standard deviation. (a) cTnI competition assay with 40 nM peptide A sample; (b) cTnT competition assay with 40 nM peptide B sample

complexes formation. The smaller standard deviations in cTnI competition assay indicate its stable and reliable read-out.

To examine whether the two (cTnI and cTnT) binding events interfere with each other in detection of corresponding protein so that this sensor can be applied in a dual detection scheme, we performed the polarization measurements for each binding in the presence of the other, shown in Figure 2.12 (a) and (b). Good linearity for both assays was still observed ($R^2=0.976$ for cTnI and $R^2=0.9677$ for cTnT). cTnI assay also kept more stable readings with smaller standard deviations. As for sensitivities, the slope of cTnI assay increased from the previous -0.0013 for single peptide assay to -0.0018 for this more complicated condition. cTnT assay has a decreased slope at -0.0009 . While keeping good linearity and sensitivities, these two measurements further demonstrated good specificity of this sensing system because little interference from each other was observed with presence of the other peptide.

Our ultimate goal is to explore whether this approach can be used for *in vitro* cTnI and cTnT detection. To achieve this objective, 10 times diluted human plasma was blended in the mixed peptide sample. Except for elevated baseline, cTnI assay kept the same good linearity ($R^2=0.9733$), sensitivity (slope= -0.0013) and relatively small error, in figure 2.13 (a). The increase in assay baseline should take into account viscosity of aqueous sample, density of molecule population, and interactions between peptides and proteins in human plasma which contains many varieties of proteins.

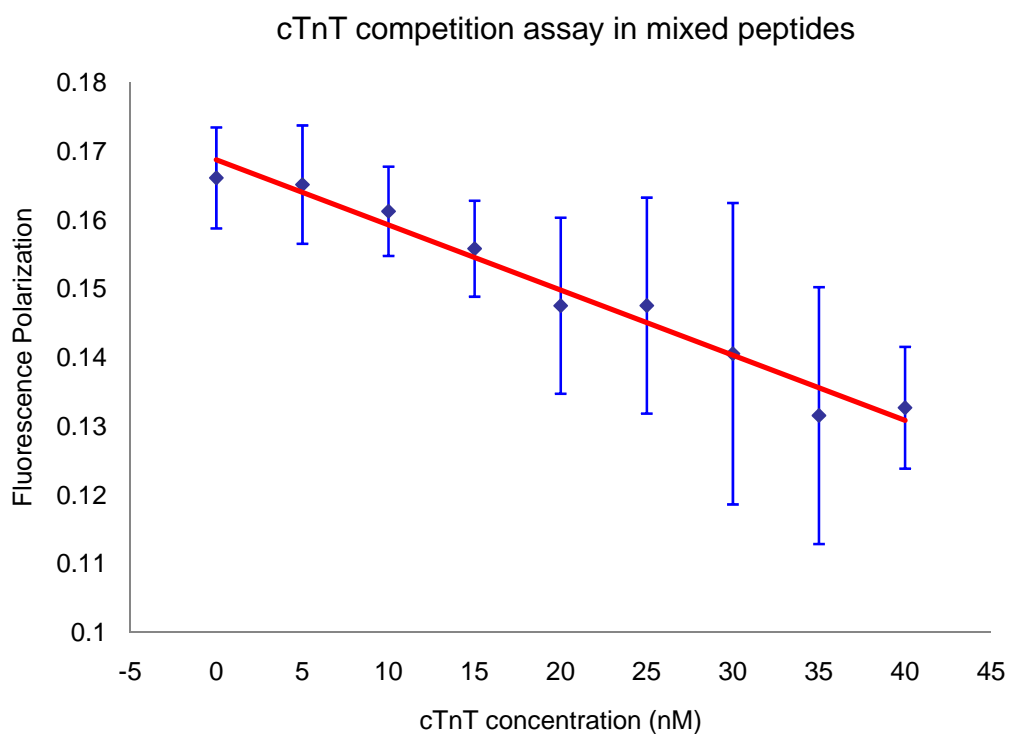
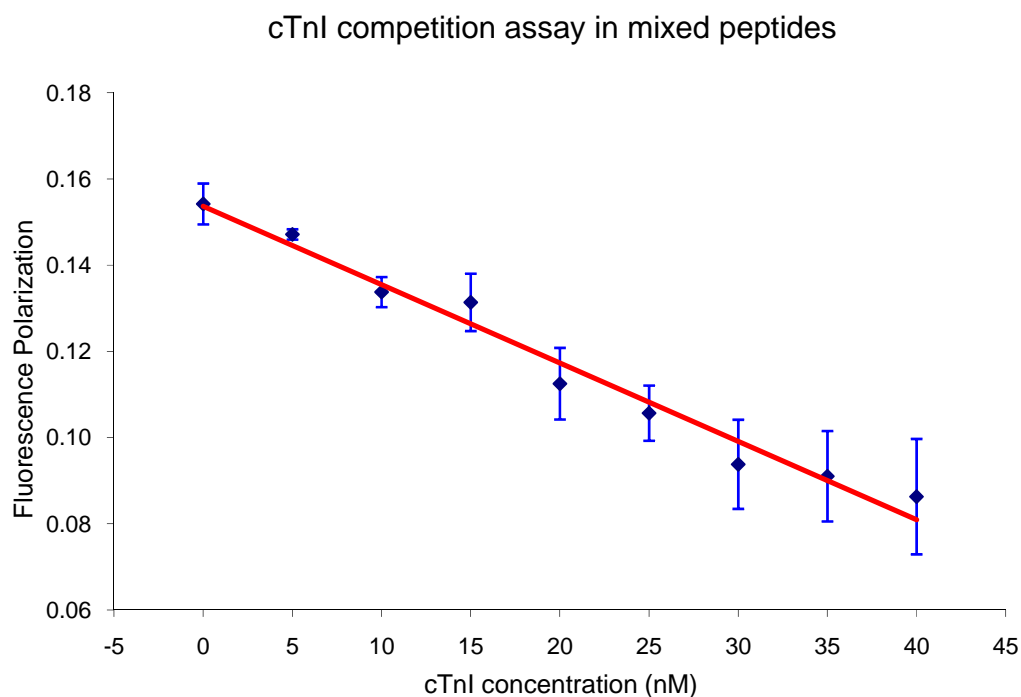


Figure 2.12 Diagrams of competition assay at mixed peptide conditions. Square dots are data points, red line is linear fitting, and error bars are standard deviation. (a) cTnI competition assay in sample which contains 40 nM peptide A and 40nM peptide B; (b) cTnT competition assay in sample which contains 40 nM peptide A and 40nM peptide B

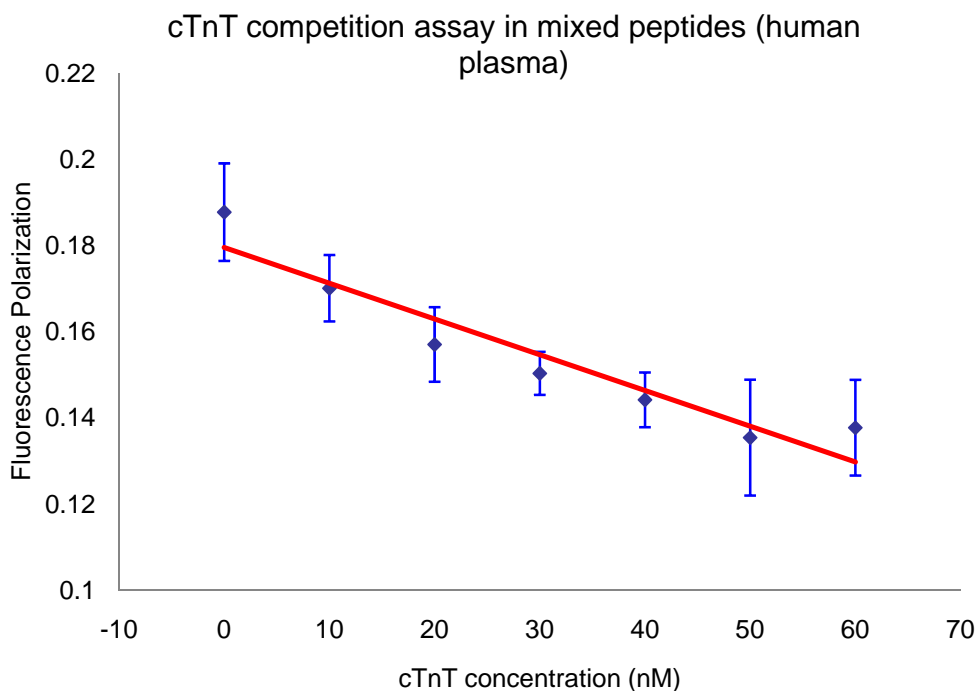
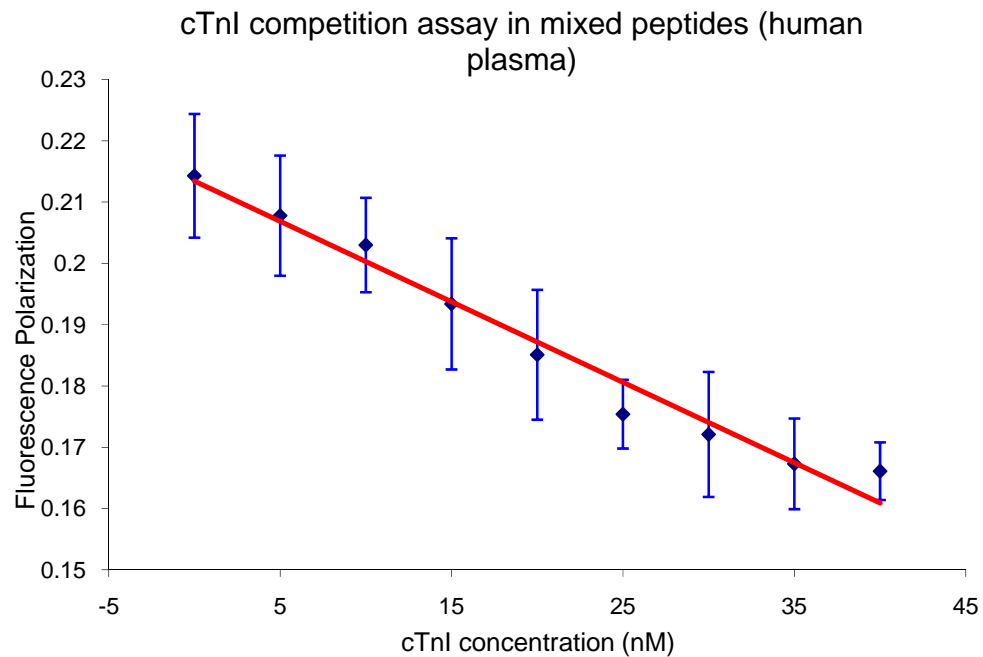


Figure 2.13 Diagrams of competition assay at mixed peptide conditions with 10 time diluted human plasma. Square dots are data points, red line is linear fitting, and error bars are standard deviation. (a) cTnI competition assay in human plasma sample which contains 40 nM peptide A and 40 nM peptide B; (b) cTnT competition assay in human plasma sample (IgG and albumin depleted) which contains 40 nM peptide A and 80 nM peptide B

Antibody-peptide B complex was more affected by the presence of various proteins in human plasma. This problem was solved by passing human plasma through an affinity column which depleted up to 95% of abundant IgG and albumin. Peptide concentration was also increased to 80 nM to give strong enough fluorescence intensity and stable FP values. After adding 60 nM full length cTnT, FP value didn't show any more decreasing trend, which indicated saturated antibodies in sample solution. Although the measurement at this particular condition is relatively demanding, its assay still showed good linearity ($R^2=0.9072$), acceptable sensitivity (slope=-0.0008) and errors, in figure 2.13 (b).

2.4 Conclusions

In the development of this novel dual-sensing scheme for simultaneous detection of two cardiac markers, cTnI and cTnT, the techniques of fluorescence polarization change at different conditions provide interesting and reliable perspectives. For all tests in either simple single peptide or complex condition mimicking *in vitro* blood sample, good linearity were demonstrated in competition assays. The broad range of FP value changes before and after adding full length protein until saturation provides good resolution, and easy and reliable measurements. All tests except the last one were carried out with 40 nM peptides; this set the sensitivity of the sensor. The measurements in mixed peptide sample and human plasma exhibit good sensing specificity and robustness. Overall, the successful demonstration of this dual-sensing system not only provides useful information on potential application of polarization measurements in clinical diagnosis

method designs, it also shows a universal approach for other protein detection as long as the monoclonal antibodies with known epitope are available.

2.5 References

- [1] Weigert, F. *Verh. d.D. Phys. Ges* 1920, *l*, 100-102
- [2] [ISS: <http://www.iss.com/resources/tech9/>]
- [3] Gryczynski, Z., Abugo, O.O., Lakowicz, J. R. "Polarization Sensing of Fluorophores in Tissues for Drug Compliance Monitoring," *Anal Biochem* 1999; 273:204-211.
- [4] Lakowicz, J. R., Gryczynski, I., Bryczynski, Z. "Novel Fluorescence Sensing Methods for High Throughput Screening," *J Biomol Screen* 2000; 5:123-131.
- [5] Mann, T. L., Krull, U. J. "Fluorescence Polarization Spectroscopy in Protein Analysis," *Analyst* 2003;128:313-317.
- [6] Lakowicz, J. R. "Principles of Fluorescence Spectroscopy," *Springer* 2006; pp12.
- [7] Ramakrishna, S. "Fluorescence Polarization Competition Immunoassay for Tyrosin Kinase," *Methods* 2000; 22:61-70.
- [8] Mann, T. L., Krull, U. J. "Fluorescence Polarization Spectroscopy in Protein Analysis," *Analyst*. 2003; 128:313-317.

Chapter 3

Sensor design based on quantum-dots fluorescence quenching by gold nano-particles

3.1 Introduction

Properties of gold nano-particles

The practical use of gold nano-particles can be dated back to the fourth century AD, and they were primarily used as pigments in glass to give a red color. Due to their tiny size, gold nano-particles are invisible to the naked eyes, but that we can tell their existence from the intense red color which results from the interaction of incident light with collective coherent oscillation of free electrons on the surface of the particles, which is known as localized surface plasmon resonance [1]. This localized surface plasmon resonance phenomenon can be observed on gold nano-particles with diameter down to 2 nm, whereas particles with diameter under this can no longer be considered as a piece of metal. The localized surface plasmon resonance of gold nano-particles is very sensitive to the composition, size, shape, inter-particle distance and dielectric properties of the environment. For example, the colloidal gold will turn blue-purple from the original red color upon aggregation to larger particles in which network is formed. For metal nanoparticles, the localized surface plasmon resonance results in an enhanced electromagnetic field at their surface, which is responsible for the extremely high extinction coefficient of the surface plasmon resonance band, with value up to $10^{11} \text{ M}^{-1}\text{cm}^{-1}$, and this is several orders of magnitude larger than those of all the organic dyes.

A traditional method to prepare colloidal gold is reducing gold (III) of chloroauric acid (HAuCl_4) by trisodium citrate dihydrate ($\text{Na}_3\text{C}_6\text{H}_5\text{O}_7 \cdot 2\text{H}_2\text{O}$) in a boiling solution. Various amounts of trisodium citrate dihydrate at different injection speed into the vortex of the boiling solution will precisely control nanoparticle sizes synthesized [2]. The surface of gold nano-particles is negatively charged because of the chemisorption of citrate ions. The colloidal gold can be prepared with size distribution ranging from 2 to 250 nm in diameter; it can be stored at room temperature and is stable over long periods of time once prepared.

Colloidal gold nano-particles have been widely used as probes in electron microscopic studies of cellular biological samples because of their high electron density. Another advantage of gold nano-particles is that they can be easily functionalized with recognition molecules such as antibodies, antigens and nucleotides by methods which lead to highly stable conjugates; this biological host-guest recognition model catalyzes the development of using gold nano-particles in imaging and sensing both *in vitro* and *in vivo*. Now global scientists have drawn great attention to gold nano-particles because of their high extinction coefficients and a broad absorption spectrum in visible light which is overlapped with the emission wavelength of commonly used fluorophores [3]. These characteristics of gold nano-particles provide them high quenching ability and make them excellent candidates as effective fluorescence energy acceptors in FRET measurements over a broad range of wavelengths.

Properties of quantum dots

The original basis of quantum dots appeared in the 1980s as quantum well. It consists of 10 nm thin layer of semiconducting material sandwiched between thicker insulating regions. When the thin layer is of the same magnitude as the wavelength of electron wave function, quantum confinement effect occurs. This constraint only happens in the direction perpendicular to this thin layer, while the other two directions are not affected. Therefore, quantum wells are also referred to as two-dimensional materials. Quantum dot, analogous to quantum well, is zero-dimensional material. That is, it confines exciton in all three directions [11]. This special structure makes quantum dot distinctive from both bulk semiconductors and discrete molecules. It also gains different optical and spectroscopic properties from traditional organic dye molecules. Therefore, quantum dots have drawn more and more attention as fluorescent probes for biological molecules.

Quantum dots are nanometer-scale semiconductor crystals; usually they are composed of cadmium selenide (CdSe) core shelled with an additional layer of Zinc sulfide (ZnS) to improve their chemical and optical properties. To facilitate its easy dispersion in aqueous solutions, this luminescent crystal material is further coated with a layer of polymer while its optical properties are retained.

Possessing distinct advantages over conventional organic dyes, quantum dots have high quantum yield, photostability, broad absorption spectra, and symmetric, size-tunable emission spectra with narrow bandwidth; the emission even can be tuned by changing the chemical composition of the crystallites. Much larger than organic dyes, the diameter of quantum dot typically ranges from 10 to 50 nm, which can be achieved by adjusting the

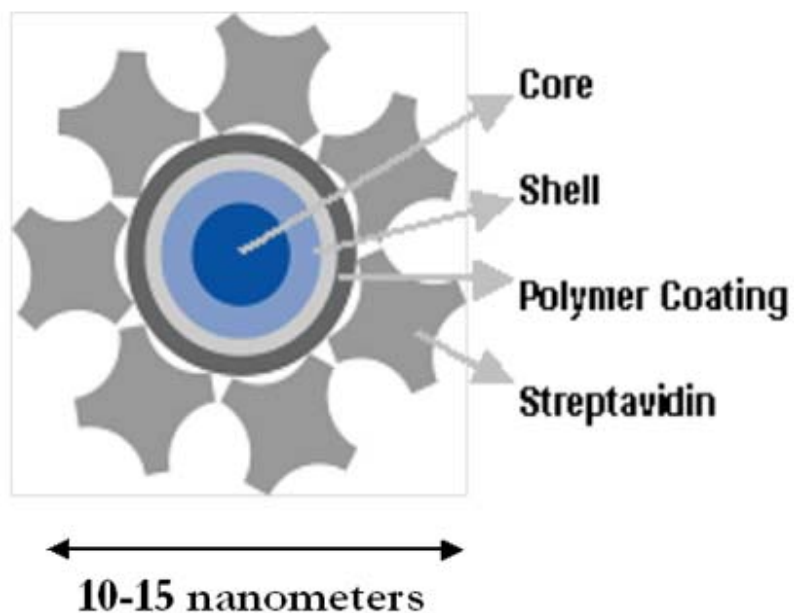


Figure 3.1 Schematic of quantum dot conjugate. Adapted from “Structure of a Qdot Nanocrystal” Invitrogen.com. <http://www.invitrogen.com/> (accessed June 16th, 2009)

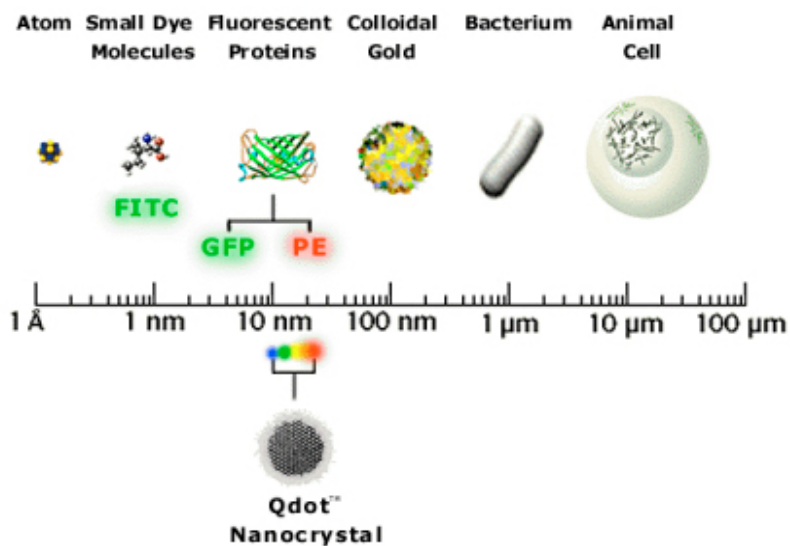


Figure 3.2 Relative sizes of quantum dots, biomolecules, colloidal gold and cells. Adapted from “Best of Nanotechnology – 2003 Awards (Best Product)” Nanotech-now.com. <http://www.nanotech-now.com/> (accessed June 16th, 2009)

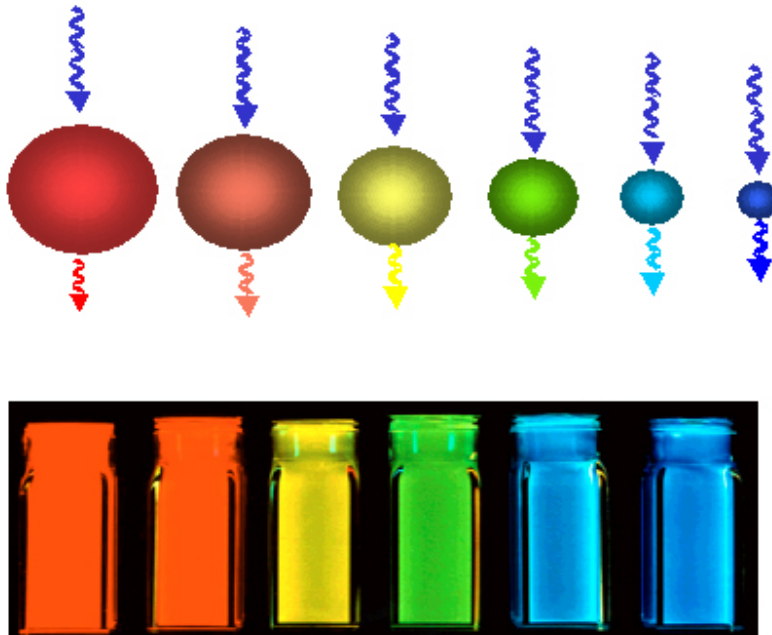


Figure 3.3 Six different size quantum dots show different color excited by a long-wave UV lamp. Adapted from “Best of Nanotechnology – 2003 Awards (Best Product)” Nanotech-now.com. <http://www.nanotech-now.com/> (accessed June 16th, 2009)

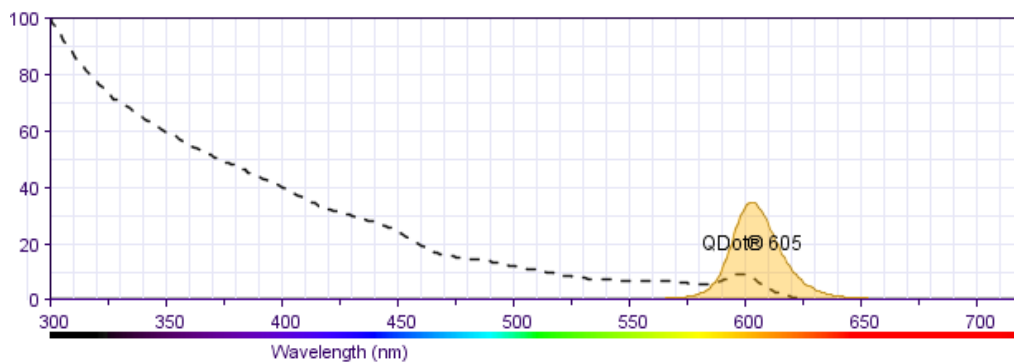


Figure 3.4 Quantum dot 605 broad excitation (dotted line) and narrow, symmetric and Gaussian-like emission spectra (shaded area), excited with 413nm laser. Adapted from “BD Fluorescence Spectrum Viewer” bdbiosciences.com <http://www.bdbiosciences.com/> (accessed June 16th, 2009)

growth time during synthesis. This size distribution is comparable to gold nano-particles and moderate size proteins. Figure 3.1 shows the structure of a typical quantum dot and biomolecule conjugate. Figure 3.2 illustrates size comparison of quantum dots, colloidal gold, proteins and other molecules. See Figure 3.3 in which the emission is tuned by changing the size of quantum dots.

Typically, the full widths at half-maximum of quantum dots' photoluminescence spectra fall in a range as narrow as 25-40 nm with symmetric Gaussian-like shape [1], which brings the potential for multiple signal detection, where many fluorescence signals can be measured simultaneously. Figure 3.4 shows the narrow, symmetric emission spectrum of Qdot 605 from Invitrogen.

Luminescent semiconductor quantum dots are effective donor fluorophores due to their high quantum yield. When brought in close proximity to dyes or quenchers such as gold nanoparticles, fluorescence of the quantum dots will be effectively quenched. This suggests that quantum dots and gold nanoparticles would be used as excellent donor-acceptor pairs to monitor protein-protein interactions. Our objective is to explore this feasibility to monitor antibody-antigen interactions using this distance-dependent quantum dot fluorescence quenching by gold nanoparticles.

Sensing schemes based on immunological interactions between antibodies and antigens are widely used because of their high sensitivity and specificity. Easy modification of the surface of both gold nano-particles and quantum dots makes this scheme even more

promising. In a typical sensing assay design, the gold nano-particles are conjugated with antibodies, and the antigens which are specific to the conjugated antibody are attached to the surface of quantum dots. Upon mixing, the interaction between the antibodies and antigens will bring the quantum dots and gold particles close to each other. We hypothesized that the close proximity between the quantum dots and gold particles would induce significant fluorescence intensity decreases, which in turn signal the recognition of antigens. In this study, instead of using antibody-conjugated gold nanoparticles and biomolecule-conjugated quantum dots, a scheme with biotinylated gold and streptavidin-labeled quantum dots has been proposed to test this sensing mechanism. Figure 3.5 illustrates the sensing scheme of this biosensor, which is based on quantum dots quenching by gold nano-particles via bioconjugation.

Streptavidin is a 52.8 kDa tetrameric protein which has very strong affinity to biotin (vitamin H). The dissociation constant (K_d) of the biotin-streptavidin complex is on the order of $\sim 10^{-14}$ mol/L, ranking among one of the strongest non-covalent interactions known in nature. These two inexpensive and easily available molecules are good substituents in simulating the specific surface recognition process of antibody-antigen interaction.

3.2 Experimental Methods

Materials and reagents

Gold colloids (5 nm, 20 nm, 30 nm) were purchased from Ted Pella, Inc. (Redding, CA). N-[6-(Biotinamido)hexyl]-3'-(2'-pyridyldithio)propionamide (Biotin-HPDP, spacer arm

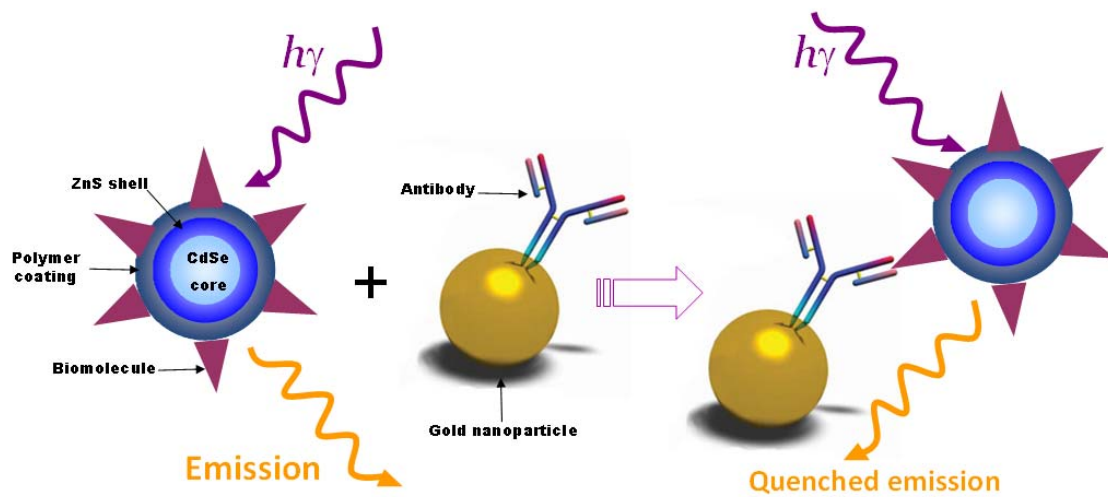


Figure 3.5 Sensing scheme based on quantum dots quenching by gold nano-particles via bioconjugation

length: 29.2 Å) (Figure 3.6) was obtained from Thermo scientific (Rockford, IL). Bovine serum albumin (BSA, reagent grade pure powder) was purchased from SeraCare Diagnostics (Milford, MA). N-Ethylmaleimide (NEM) was purchased from PIERCE (Rockford, IL). Qdot streptavidin conjugates were purchased from Invitrogen (Carlsbad, CA). 5 nm, 20 nm, 30 nm Biotin labeled gold nanoparticles (5-10 biotin molecules per particle) were purchased from Nanocs Inc. (New York, NY). Sodium cyanide was obtained from J.T. Baker (Phillipsburg, NJ).

Buffer preparation

Quenching of fluorescence involving protein and ligand is complicated to implement because of the existence of electrostatic forces between exposed areas on the negative charged gold particles and cationic structures within the protein. Therefore, the proteins have a tendency to adsorb on gold surface via non-specific interactions. [4] To minimize this nonspecific binding, incubation step can be included in which a noncompeting protein which has high affinity to gold particles is used. These proteins (e.g., bovine skin gelatin, fish gelatin, and BSA) can occupy and cover protein-reactive areas, hence decreasing electrostatic interactions between the target proteins and the exposed surface areas on gold particle. [5]

To reduce non-specific binding in our work, commercially available bovine serum albumin (BSA) has been introduced as one of the main buffer components to mask these exposed surfaces. To keep the gold nano-particles stable in solution, low salt condition (10 mM phosphate buffer, pH=7.5) is used.

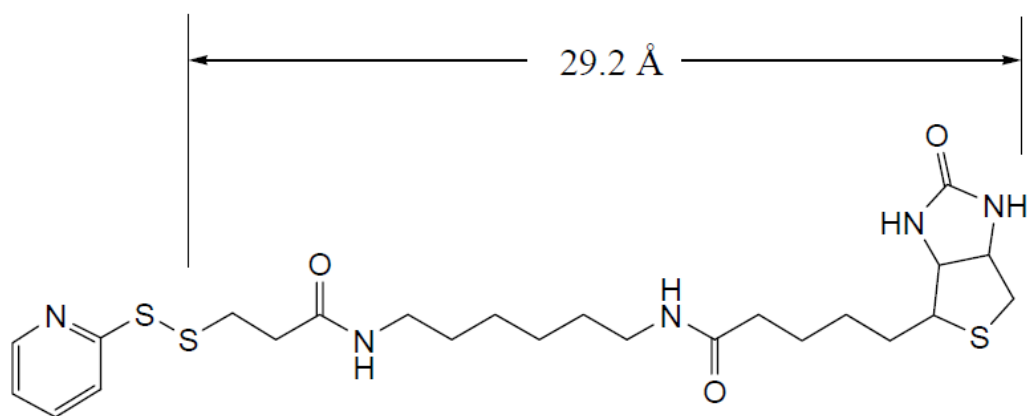


Figure 3.6 Chemical structure of biotin-HPDP. From Thermo Scientific product instruction #21341 EZ-link Biotin-HPDP

Blocking of BSA surface cysteines

In our design, chemical biotin-HPDP was used for biotinylation of gold nano particles. Though BSA was used as an excellent blocker to cover the exposed surface areas of the gold nano particles, there are free sulfhydryls on the surface of BSA which are reactive to the disulfide bond [6] of biotin-HPDP. Therefore, it is necessary to deactivate the surface sulfhydryls to guarantee easier access of biotin molecules to the surface of gold nano-particles and not being trapped by BSA.

N-Ethylmaleimide (NEM) is an alkylating reagent that reacts with sulfhydryls and forms stable thioether bonds. In this reaction, pH plays an important role in determining which specific functional group to be modified. At pH 6.5-7.5, the maleimide reaction is specific for sulfhydryls, whereas reactivity with amino groups occurs at pH higher than 7.5. Maleimide groups react with sulfhydryls by nucleophilic attack of the thiolate anion on one of the carbons of the double bond. When sufficient sulfhydryls have been blocked, the reaction can be monitored by the decrease in absorbance at 300 nm as the double bond becomes a single bond. The resulting thioether group is non-reversible and terminates in an ethyl group, blocking or capping the sulfhydryl.[7,8]

Dissolve BSA to be blocked in Phosphate Buffered Saline (PBS, 100 mM NaH₂PO₄, 100 mM Na₂HPO₄, 150 mM NaCl, pH=7.2) at 10 mg/ml (1% w/v). Equilibrate NEM to room temperature before opening to prevent condensation in the bottle and subsequent hydrolysis and thus loss of function. To prevent hydrolysis of the maleimide group, prepare 200 mM of NEM stock solution in ultrapure water immediately before use. Add

15-fold molar excess of NEM to sulfhydryl groups to be blocked. Stir for 2 hours at room temperature. Dialyze blocked BSA (NEM-BSA) in 10mM phosphate buffer (pH=7.5) to remove excess NEM.

Observe colloidal gold with transmission electron microscopy

To check the size distribution of the purchased colloidal gold which is to be biotinylated, 15 nm colloidal gold from Ted Pella, Inc. is observed under TEM. The gold is in the original condition which is in water. Sample is prepared by pipetting 5 μl colloidal gold ($227 \text{ particles}/\mu\text{m}^3$) onto carbon coated grid followed by drying it under the lamp.

Biotinylation of gold nano particles (GNP)

Discard water from original colloidal gold by centrifugation: 8 min @ 13K rpm for 30 nm GNP, 15 min @ 13K rpm for 20 nm GNP, 80 min @ 13K rpm for 5 nm GNP. Dissolve biotin-HPDP in DMSO to make 4 mM stock solution. Add a certain volume of biotin-HPDP to NEM-BSA phosphate buffer first, then add concentrated GNP and stir the sample at room temperature overnight. Centrifuge twice to get rid of unreacted excess biotin-HPDP, followed by resuspending GNP in NEM-BSA phosphate buffer.

Test of fluorophores quenching

Concentration of biotinylated GNP was measured with Beckman UV/Vis spectrophotometer and calculated using the extinction coefficients provided in product data sheet. Then the biotinylated GNP was diluted with NEM-BSA phosphate buffer to

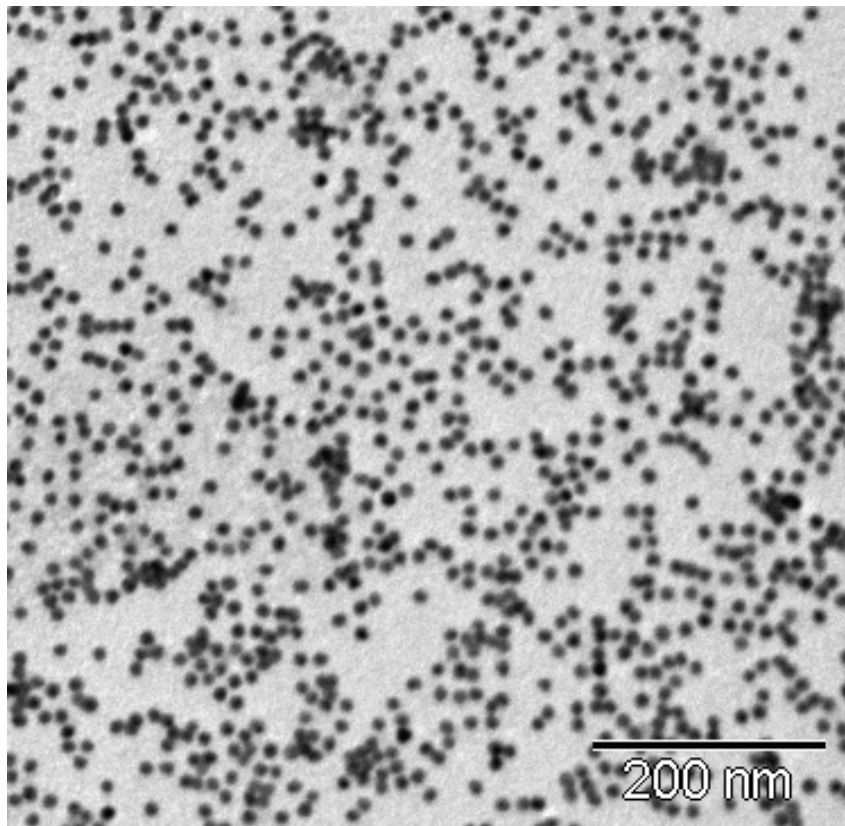


Figure 3.7 Transmission electron micrograph of gold nano-particles (15 nm, from Ted Pella Inc.)

desired concentrations. Add 0.033 nM Qdot® 605 streptavidin conjugates (SQ605) to 1.2 ml of the prepared sample solution in a 3ml standard quartz cuvette (1 cm path length). Fluorescence intensities of quantum dot in the sample solutions with either bare gold nano-particles or biotinylated gold nano-particles were measured at different conditions at 10 °C on ISS PC1 photon-counting spectrophotometer. SQ605 is excited at 400 nm with 500 nm cut-off filter applied to the emission end.

3.3 Results and discussion

Colloidal gold size distribution under TEM

The size distribution of GNP is acceptably uniform, shown in Figure 3.7. Some aggregated parts seen in the view may be formed in the drying step during sample preparation. These well-separated and uniformly-distributed GNP are suitable for subsequent biotinylation and quantum dot quenching experiments.

BSA surface sulfhydryls blocking by NEM

To check the BSA surface modification with NEM, the reaction kinetics of sulfhydryls and maleimide group was investigated first. This reaction took two hrs and was monitored with Beckman Coulter DU730 life science UV/Vis spectrophotometer. The data obtained was replotted and shown in Figure 3.8. The linearly-decreasing absorbance at 300 nm suggests that the double bond of maleimides underwent an alkylation reaction with sulfhydryl groups in BSA surface cysteine to form stable thioether bonds. After changing buffer to optimum biotinylation condition, BSA with successfully-deactivated surface cysteines is good protector for gold nano-particles without trapping biotins.

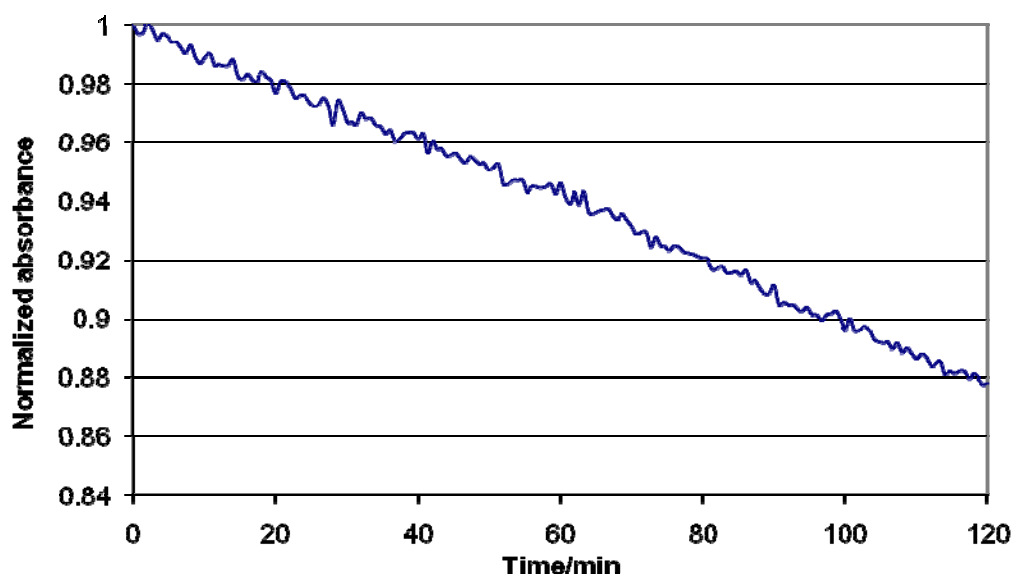


Figure 3.8 Kinetics of *BSA* surface sulfhydryls blocking by NEM. The decreased absorbance is evidence of double bonds breaking down

Biotinylation of gold nano-particles (GNP)

As shown in Figure 3.9, the surface plasmon resonance peak of the bare gold nano-particles occurred at 523 nm, while upon the chemisorption of biotin-HPDP molecules, the surface plasmon resonance band was broadened and underwent a redshift to 530 nm, which was caused by the formation of dielectric layers around the colloidal gold. [10] The biotin-HPDP molecules functionalized on the surface of gold nanoparticles have extended spacer arm in the chemical structure which helps reduce steric hindrance and reach the biotin binding sites on streptavidin more easily, thus helping to increase the sensitivity in detecting streptavidin-conjugated quantum dots.

When the colloidal gold has inter-particle distance substantially larger than average particle size, the color of colloidal gold is red. But with the decrease of inter-particle distances to approximately average particle sizes, gold colloidal will give a blue color. [9] This is what happens during the biotinylation. As shown in Figure 3.10, with the increase of biotin-HPDP concentration during the incubation of the mixtures of GNP and biotin-HPDP, the color of biotinylated gold nano particles was seen to gradually turn blue from its original red color. The negative charge on the surface of gold nano-particles is responsible for keeping the good dispersivity of colloidal gold and also maintaining the red color of the solution. Upon the complex formation between biotin-HPDP and gold nano-particles, the existence of attached biotin molecules partially neutralized the negative charge on gold surface, which brought previously well-dispersed gold nano-particles closer to each other. Therefore, the color got darker during biotinylation.

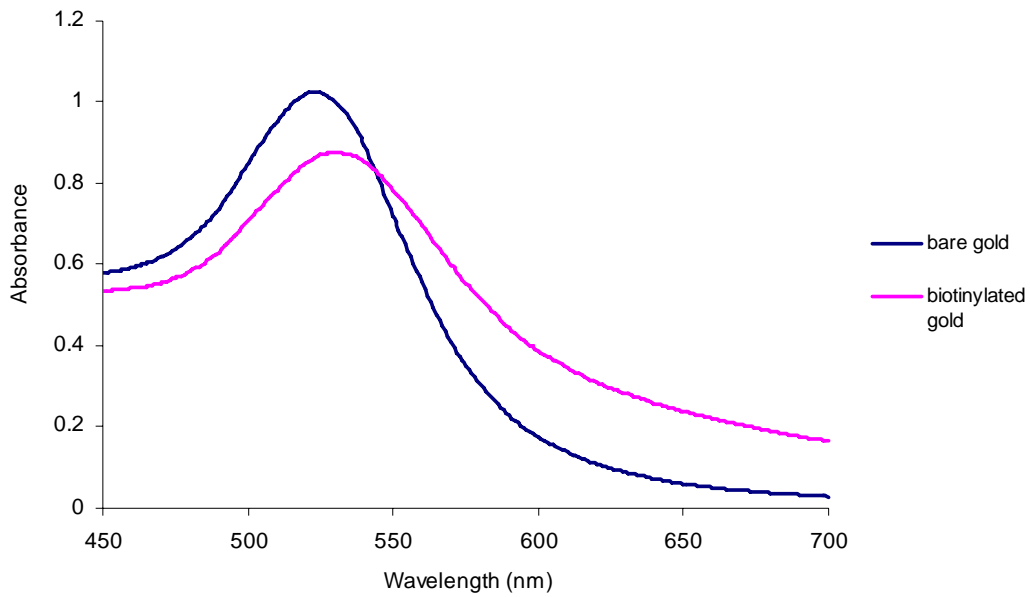


Figure 3.9 Absorption spectrum of 20 nm bare gold nano particles and 20nm biotinylated gold nano particles. The surface modification on nano-gold by biotin changes the wavelength of maximum absorption from 523 nm to 530 nm

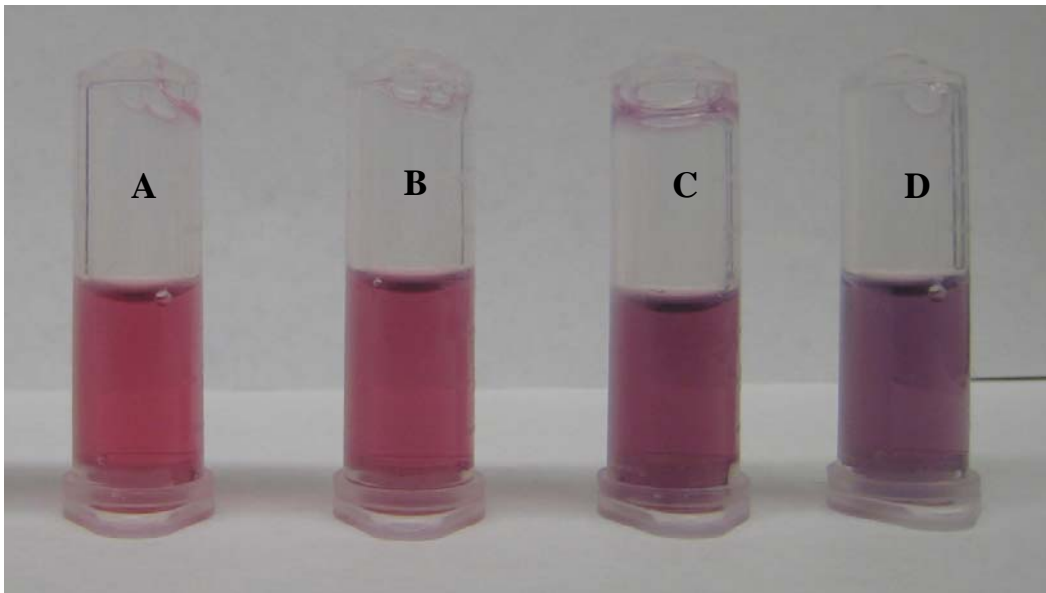


Figure 3.10 Color comparison of different biotin-HPDP vs. gold nano-particles ratio in biotinylation (samples vary in biotin-HPDP concentration used in biotinylation step). A. 5 μ M biotin-HPDP; B. 10 μ M biotin-HPDP; C. 20 μ M biotin-HPDP; D. 40 μ M biotin-HPDP

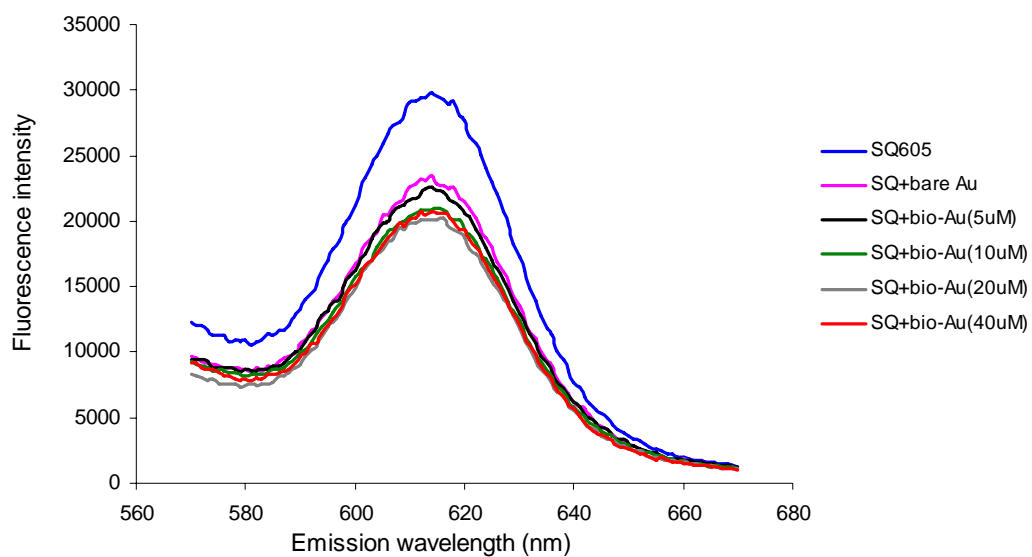


Figure 3.11 Biotin-HPDP concentration effects on the fluorescence quenching efficiency; here 20 nm gold nano particles were used. As shown in the figure, at 20 μ M biotin-HPDP concentration, best quenching is seen - about 50% of the original fluorescence from SQ605 is quenched

High ratio of biotin-to-gold nano-particle enables more binding of quantum dot labeled streptavidin leading to better quenching of fluorescence. However, the high ratio may affect the stability of biotinylated colloidal gold in solution. So the goal of this experiment was to define the critical biotin-to-gold ratio which can lead to high quenching and maintain good dispersivity of biotinylated colloidal gold. The results of quenching experiments are shown in Figure 3.11. Increasing biotin-HPDP concentration used in the biotinylation to 20 μM consistently improves quenching efficiency steadily. However, increasing the biotin-HPDP concentration to 40 μM made no further improvement to the fluorescence quenching efficiency. Furthermore, even in the presence of NEM-BSA to stabilize the dispersivity of the gold colloids in solution, the high concentration (40 μM) of the biotin-HPDP made the colloid unstable. The red gold colloids became irreversible black precipitins. This irreversible gold aggregation process indicates that too many ligands on the surface have been attached and they neutralize most of the negative charge so the distance between particles decreases to “unsafe” range in which good dispersivity is no longer maintained.

Test of Quenching Efficiency

We also investigated the effects of the size of Gold nano particles on quantum dot fluorescence quenching (Figure 3.12). The results suggest that size of gold nano particles plays an important role in quenching SQ605 when all the other conditions were kept the same. This is clearly shown in Figure 3.12 (b), where the ratio of biotinylated GNP over SQ605 was kept at 5:1 in measurement and the SQ605 was excited at 400 nm. While 5nm biotinylated GNP quenched about 6% of total fluorescence, the quenching

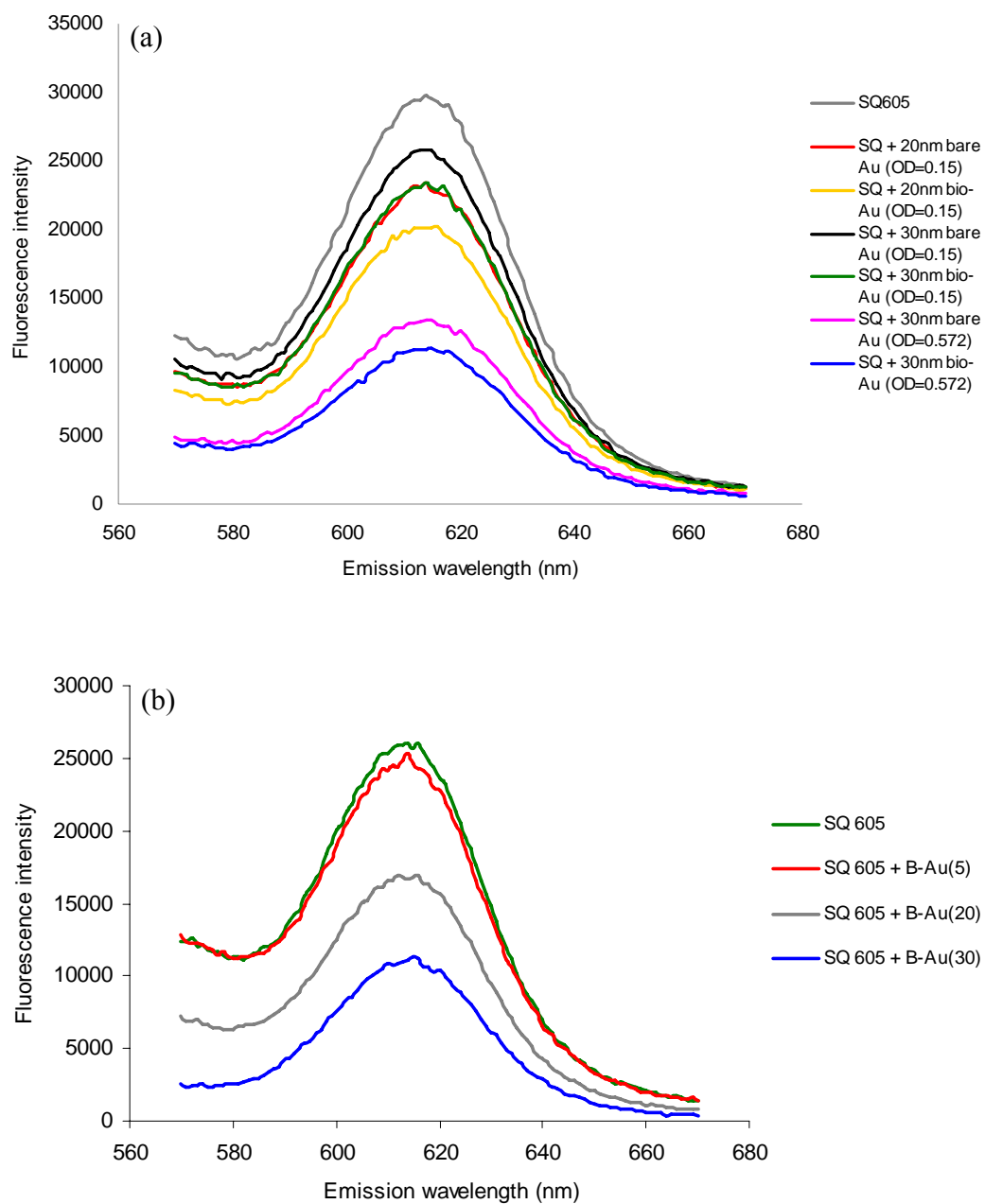


Figure 3.12 Gold nano-particle size effects [lab made (a) and purchased] on fluorescence quenching efficiency

efficiency increased to 36% for 20 nm GNP, to about 58% for 30 nm GNP. These results were further confirmed with lab made biotinylated GNP. In Figure 3.12 (a), when the concentrations for both 20 nm and 30 nm biotinylated gold particles were kept the same, these two sizes of GNP showed similar quenching efficiencies as purchased GNP. This can be explained that although there were same amount of particles in the sample, 30 nm GNP have larger surface area to quench fluorescence.

An interesting phenomenon was seen from all the quenching measurement was that fluorescence intensity of quantum dot was decreased even in the presence of bare gold particles. This phenomenon is mainly caused by inner filter effect which is an apparent decrease in emission quantum yield as a result of reabsorption of emitted radiation by a species other than the intended primary absorber, GNP themselves in our case. To see how much contribution of this inner filter effect made in quenching measurements, we compared fluorescence quenching from both 20 nm and 30 nm biotinylated gold particles while keeping the optical density of both size particles at 0.15 OD. The gold particles with 20 nm size showed higher quenching efficiency. That observation can be explained that it has smaller extinction coefficient ($\epsilon = 9.406 \times 10^8 \text{ M}^{-1}\text{cm}^{-1}$ of 20 nm nano gold particle compared to $\epsilon = 3.585 \times 10^9 \text{ M}^{-1}\text{cm}^{-1}$ of 30 nm nano gold particle), thus higher concentration.

To check the role of BSA molecules in protecting and stabilizing colloidal gold, quenching measurements of 20 nm biotinylated GNP in different diluted NEM-BSA buffer were performed. As shown in Figure 3.13, BSA molecules did play a surfactant

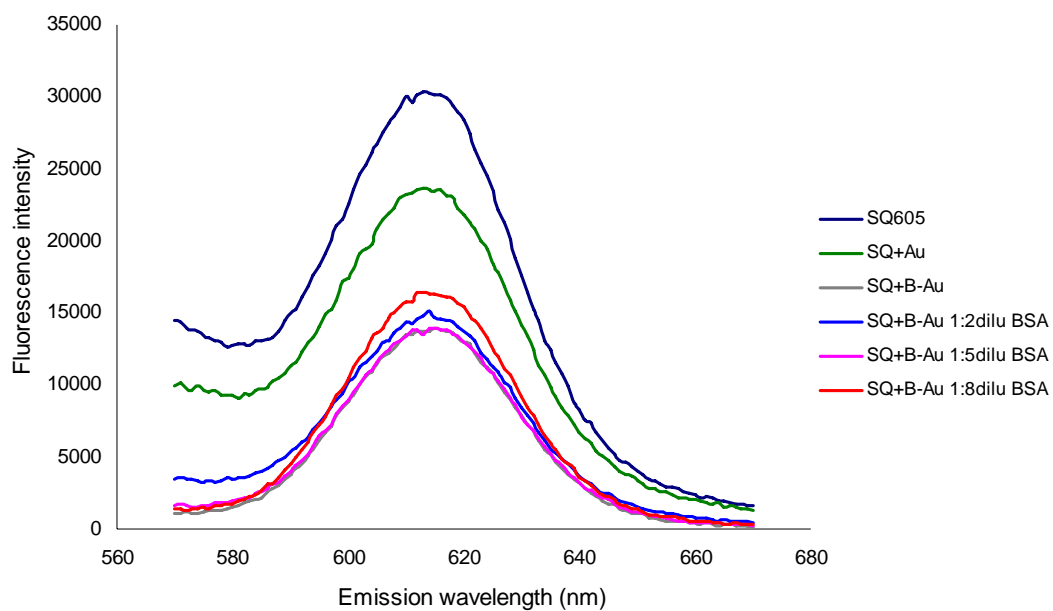
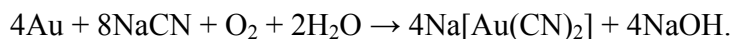


Figure 3.13 Effects of NEM-BSA phosphate buffer dilution on the fluorescence quenching efficiency

role in the buffer system since the test in undiluted buffer gave the best quenching, while the most diluted gave the worst.

Fluorescence recovery

To verify quenching of GNP on quantum dot fluorescence, a quenching measurement with sodium cyanide was carried out. This chemical is mainly used in gold and other precious metal mining, and the reaction involved with gold is shown below:



As shown in Figure 3.14, adding NaCN to the previously-quenched sample led to significant recovery of the quenched fluorescence because gold was oxidized and lost its suppression on the fluorescing SQ605.

Varying ratio of biotinylated GNP and SQ605

To examine effects of GNP concentrations on SQ605 fluorescence quenching, we performed fluorescence quenching measurements at different GNP to SQ605 ratio. In our quenching measurements, SQ605 was diluted to 0.033 nM, while concentrations of biotinylated gold nanoparticles (30 nm) were varied from 0.033 nM to 0.165 nM. This gave the ratio of SQ605 to GNP from 1:1 to 1:5. With excitation at 400nm, the measurements were performed at 10 °C. As shown in Figure 3.15, more fluorescence from SQ605 was quenched with higher concentration of biotinylated gold nano-particles. This confirmed the success biotinylation of GNP and GNP's quenching abilities on SQ605.

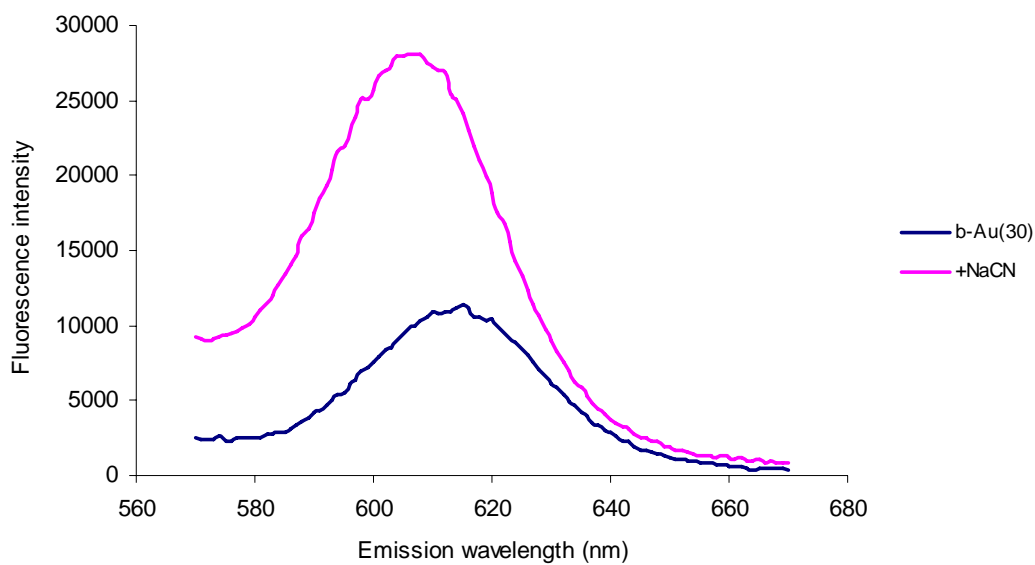


Figure 3.14 Fluorescence recovery after adding sodium cyanide

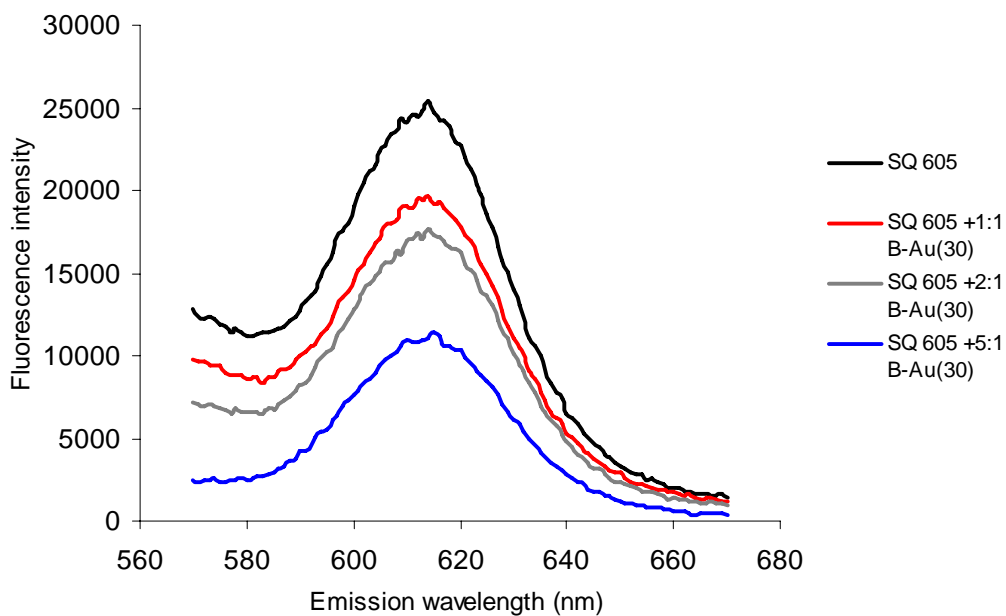


Figure 3.15 Quenching test with different ratios of biotinylated GNP over SQ605

3.4 Conclusions

In summary, the sensing scheme of quenched quantum dots by gold nano-particles has been tested in a simplified mode with strong binding of biotin and streptavidin. With the protection and stabilization by NEM-modified bovine serum albumin, quenching efficiency of biotinylated gold nano-particles on streptavidin-conjugated quantum dots 605 were tested with various gold particles to quantum dot ratio, different sizes of gold particles, and different concentration biotinylated GNP. The results showed that GNP have strong quenching ability on SQ605 via immunobinding between biotin and streptavidin, which makes it possible to apply this sensing scheme to more complicated and practical settings with antibody and antigen. One problem that needs to be further addressed is the inner filter effect's contribution in fluorescence quenching. But with the control of bare GNP, this sensing system still works as effective detector of target analytes.

3.5 References

- [1] Oh, E., Hong, M.Y., Lee, D., Nam, S.H., Yoon, H.C., Kim, H.S. "Inhibition Assay of Biomolecules Based on Fluorescence Resonance Energy Transfer (FRET) between Quantum Dots and Gold Nanoparticles," *J Am Chem Soc* 2005; 127(10):3270.
- [2] Wilson, R. "The Use of Gold Nanoparticles in Diagnostics and Detection," *Chem Soc Rev* 2008; 37:2028-2045.
- [3] Drozdowicz, T. K. et al. "Depolarized Light Scattering from Colloidal Gold Nanoparticles," *Chemical Physics Letters* 2009; 468:69–74.
- [4] Hayat, M.A. et al. "Colloidal Gold: Principles, Methods, and Applications," Academic Press: San Diego, CA, 1991

- [5] Matthias, K., Matthew, B. Z., “Photothermal Readout of Surface-arrayed Proteins: Attomole Detection Levels with Gold Nanoparticle Visualization,” *J Phys Chem B* 2005; 109:16736-16743.
- [6] Netto, L.E.S. et al. “Reactive Cysteine in Proteins: Protein Folding, Antioxidant Defense, Redox Signaling and More,” *Comparative Biochemistry and Physiology* 2007; 146:180–193.
- [7] Smyth, D.G., et al. “Reactions of *N*-ethylmaleimide,” *J Am Chem Soc* 1960; 82:4600.
- [8] Brewer, C.F., Riehm, J.P. “Evidence for Possible Nonspecific Reactions Between *N*-ethylmaleimide and Proteins,” *Anal Biochem* 1967; 18:248.
- [9] Thanh, N. T. K., Rosenzweig, Z. “Development of an Aggregation-based Immunoassay for Anti-protein A Using Gold Nanoparticles,” *Anal Chem*, 2002;74:7 .
- [10] Aslan, K., Lakowicz, J.R., Geddes, C. D. *Anal Biochem* 2004; 330:145.
- [11] Norris, D.J. “Measurement and Assignment of the Size-dependent Optical Spectrum in Cadmium Selenide (CdSe) Quantum Dots”, thesis, presented to Massachusetts Institute of Technology at Cambridge, MA, in partial fulfillment of the requirements for the degree of Doctor of Philosophy (1995).

Chapter 4

Summary

Conclusions

The work presented in this thesis includes two research projects. The first is the exploration of a sensing assay design to simultaneously detect two biomarkers – cardiac troponin I and cardiac troponin T, based on peptide competition assay by monitoring fluorescence polarization changes. The other project is to explore the feasibility of implementing FRET approach in a sensing scheme to monitor protein-protein binding events using quantum dots as fluorescent donors and gold nano-particles as quenchers. Both sensing designs utilize immunological interaction as the recognition method due to its high sensitivity and specificity.

In the first sensing mode, peptide competition assays were performed at three different conditions with increasing complexity on a final attempt to mimic the *in vitro* blood sample test conditions. All six competition assays showed linear changes in fluorescence polarization with the presence of increasing amount of target cardiac marker, either cTnI or cTnT. Although the cTnT peptide competition assay in human plasma needs an additional step of sample treatment to reduce the strong bulk protein background, all the measurements have collectively demonstrated good specificity, sensitivity and robustness for this dual-sensing system.

In the second scheme, protocol procedures for gold nano-particle biotinylation were successfully developed, and optimized condition was also established to achieve more

than 50% quenching of total fluorescence. Our results based on the simplified high affinity binding between biotin and streptavidin suggest that this sensing scheme is effective and can be developed into a sensor for monitoring antibody and antigen interactions.

Future directions

The ultimate goal of this research project is to identify a suitable and applicable sensor design for cardiac marker detection at patients' convenience. Therefore, for fluorescence polarization sensor design, more work needs to be done in fine tuning the system, in peptide design, fluorophore screening and instrumental modification to increase sensitivity of cTnI and cTnT detection in the blood samples. For quantum dot and gold colloid FRET sensing design, our results suggest that excellent optical and chemical properties of quantum dots make multiplex analytes sensing mode possible. More experiments need to be done in optimizing sensing design to make multiple sensing possible.